Moho depth across the Trans-European Suture Zone from *P*- and *S*-receiver functions

Brigitte Knapmeyer-Endrun,* Frank Krüger and the PASSEQ Working Group†

University Potsdam, Institute of Earth and Environmental Sciences, Karl-Liebknecht-Str. 24-25, D-14476 Potsdam, Germany. E-mail: endrun@mps.mpg.de

SUMMARY

The Mohorovičić discontinuity, Moho for short, which marks the boundary between crust and mantle, is the main first-order structure within the lithosphere. Geodynamics and tectonic evolution determine its depth level and properties. Here, we present a map of the Moho in central Europe across the Teisseyre-Tornquist Zone, a region for which a number of previous studies are available. Our results are based on homogeneous and consistent processing of *P*- and *S*-receiver functions for the largest passive seismological data set in this region yet, consisting of more than 40 000 receiver functions from almost 500 station. Besides, we also provide new results for the crustal v_P/v_S ratio for the whole area.

Our results are in good agreement with previous, more localized receiver function studies, as well as with the interpretation of seismic profiles, while at the same time resolving a higher level of detail than previous maps covering the area, for example regarding the Eifel Plume region, Rhine Graben and northern Alps. The close correspondence with the seismic data regarding crustal structure also increases confidence in use of the data in crustal corrections and the imaging of deeper structure, for which no independent seismic information is available.

In addition to the pronounced, stepwise transition from crustal thicknesses of 30 km in Phanerozoic Europe to more than 45 beneath the East European Craton, we can distinguish other terrane boundaries based on Moho depth as well as average crustal v_P/v_S ratio and Moho phase amplitudes. The terranes with distinct crustal properties span a wide range of ages, from Palaeoproterozoic in Lithuania to Cenozoic in the Alps, reflecting the complex tectonic history of Europe. Crustal thickness and properties in the study area are also markedly influenced by tectonic overprinting, for example the formation of the Central European Basin System, and the European Cenozoic Rift System. In the areas affected by Cenozoic rifting and volcanism, thinning of the crust corresponds to lithospheric updoming reported in recent surface wave and *S*-receiver function studies, as expected for thermally induced deformation. The same correlation applies for crustal thickening, not only across the Trans-European Suture Zone, but also within the southern part of the Bohemian Massif.

A high Poisson's ratio of 0.27 is obtained for the craton, which is consistent with a thick mafic lower crust. In contrast, we typically find Poisson's ratios around 0.25 for Phanerozoic Europe outside of deep sedimentary basins. Mapping of the thickness of the shallowest crustal layer, that is low-velocity sediments or weathered rock, indicates values in excess of 6 km for the most pronounced basins in the study area, while thicknesses of less than 4 km are found within the craton, central Germany and most of the Czech Republic.

Key words: Body waves; Cratons; Crustal structure; Europe.

GJI Seismology

1 INTRODUCTION

The Moho is the major first-order discontinuity within the lithosphere. As it separates the chemically highly differentiated crust from the more homogeneous upper mantle, its depth level and sharpness are strongly related to the tectonic and geodynamic evolution of the considered area. The study of Moho topography can thus aid in understanding tectonic developments and dynamics of the lithosphere. From a more applied point of view, detailed information on the Moho depth is needed for example in gravimetric modelling, for precise localization of local earthquakes, interpretation of heat flow data, and crustal corrections in teleseismic tomography, the calculation of *P*-wave residual spheres and depth estimation of deeper discontinuities (e.g. the lithosphere-asthenosphere boundary or the upper mantle discontinuities) from receiver functions (RFs).

The geology of central Europe reflects its long tectonic evolution (Fig. 1). Current surface geology and crustal lithology indicate a major contrast between the area to the north and east of the Sorgenfrei-Tornquist Zone (STZ) and the Teisseyre-Tornquist Zone (TTZ), which consists of a basically homogeneous block, the palaeocontinent Baltica, and the more complex situation in Phanerozoic Europe to the west. These two linked zones, the TTZ to the east of the island of Bornholm and the STZ to the west, mark the southwestern boundary of the Precambrian East European Craton (EEC). Southwest of them lies a 150–200 km wide region of suspect terranes, the Trans-European Suture Zone (TESZ, Dadlez *et al.* 2005).
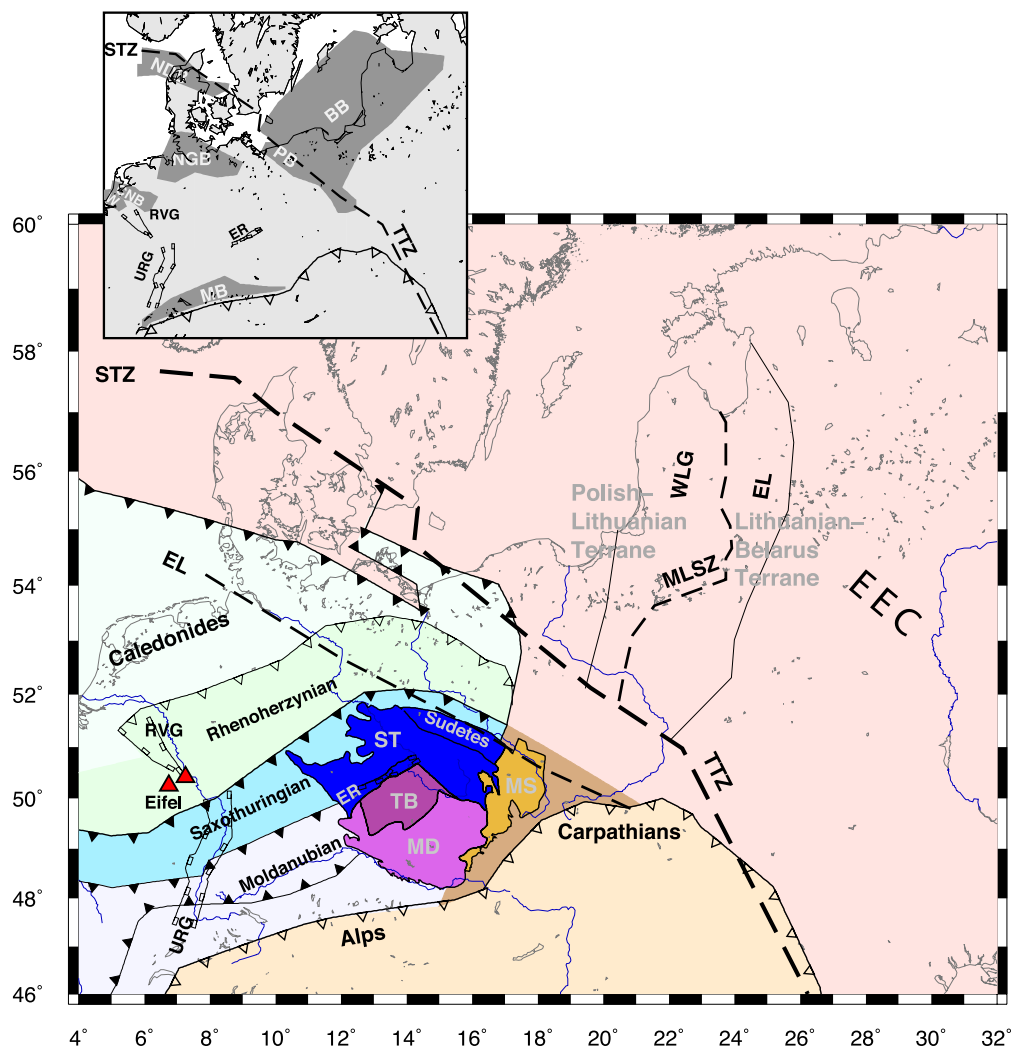

Figure 1. Simplified tectonic map of the study region in central Europe after Pharaoh *et al.* (2006) and Kroner *et al.* (2008). Filled ticks denote oceanic sutures, open ticks orogenic frontal zones. The outlines of the Bohemian Massif, indicated by brighter colours, and its individual units are taken from Plomerová *et al.* (2005). Boundaries of Upper Rhine Graben and Roer Valley Graben are drawn after Reicherter *et al.* (2008), Mid-Lithuanian Suture Zone and units within Lithuania after Kozlovskaya *et al.* (2001). Red triangles outline Quarternary volcanic activity in the Eifel region (Litt *et al.* 2008) . Inset shows the locations of the main basins within the study area (van Balen *et al.* 2000; Dadlez *et al.* 1995, 2005; Nikishin *et al.* 1996), together with grabens of the European Cenozoic Rift System and the Alpine deformation front. Key to labels: BB, Baltic Basin; CNB, Central Netherlands Basin; EEC, East European Craton; EL, East Lithuanian Belt; ER, Eger Rift; MB, Molasse Basin; MD, Moldanubian of Bohemian Massif; MLSZ, Mid-Lithuanian Suture Zone; MS, Moravo-Silesian of Bohemian Massif; NDB, North Danish Basin; NGB, North German Basin; PB, Polish Basin; RVG, Roer Valley Graben; ST, Saxothuringian of Bohemian Massif; STZ, Sorgenfrei-Tornquist Zone; TB, Tepla-Barrandian of Bohemian Massif; TTZ, Teisseyre-Tornquist Zone; URG, Upper Rhine Graben; W, West Netherlands Basin; WLG, West-Lithuanian Granite Domain.

Geophysical investigations with various methods have shown that the STZ-TTZ is not merely a surficial feature, but extends into the lithosphere (e.g. Schweitzer 1995; Yegorova & Starostenko 1999; Banka *et al.* 2002; Korja 2007; Koulakov *et al.* 2009; Majorowicz & Wybraniec 2011; Legendre *et al.* 2012; Zhu *et al.* 2012), consistent with the tectonic evolution of central Europe. Whereas Baltica as a part of the EEC has been stable for at least 1.45 Ga (Bogdanova *et al.* 2006), Phanerozoic central Europe is made up of a number of continental fragments that have been rifted off the palaeoconti-nent Gondwana and accreted to Baltica during consecutive oroge-nies (Pharaoh 1999; Winchester & the PACE TMR Network Team 2002). From north to south and oldest to youngest, amalgamation occurred during the late Ordovician Caledonian orogeny, the late Silurian to early Carboniferous Variscan orogeny and the Cretaceous to Cenozoic Alpine-Carpathian orogeny (Fig. 1). The crystalline basement of the Variscan orogen in Central Europe is prominently exposed in the Bohemian Massif (BM), featuring high-pressure to ultra-high pressure rock suites. The BM consists of different tectonic units, corresponding to the remains of microplates and magmatic arcs accreted during subduction and continental collision (Schulmann *et al.* 2009). From north-west to south-east, the main units are the Saxothuringian, Tepla-Barrandian and Moldanubian domains, whereas the Sudetes mountains and the Moravo-Silesian terrane are located to the east (e.g. Plomerová *et al.* 2012, Fig. 1).

Traces of subduction during the most recent orogenies can still be imaged as high-velocity slab anomalies in seismic tomography beneath the Alps and Carpathians (e.g. Lippitsch *et al.* 2003; Zhu *et al.* 2012). Similar evidence for the older orogenies is missing due to significant overprinting and tectonic reworking. Extension and subsidence associated with the collapse of the Variscan orogeny in Permian to Mesozoic times resulted in the formation of deep sedimentary basins, the Central European Basin System, along the southwestern margins of the EEC (Dadlez *et al.* 1995). The Polish Basin, located on top of the TESZ, is its eastern-most member. Low *P*-wave velocities associated with sediments have been detected down to 16–20 km depth within this basin (Grad *et al.* 2003a). The Variscan part of central Europe was also strongly affected by the spreading of the European Cenozoic Rift System in response to in-traplate compression caused by the collisional tectonics in the Alps and Pyrenees (Dézes *et al.* 2004; Prodehl *et al.* 2006). Grabens in central Europe associated with the European Cenozoic Rift System include the Massif Central–Rhône Valley, the Rhine Graben, the Rhenish Massif and the Eger Rift within the BM (Fig. 1). Rifting, which was accompanied and partly preceded by widespread alka-line volcanism, started during the late Eocene in these areas (Ziegler 1994; Dézes *et al.* 2004). Besides, flexural subsidence in the north-ern foredeep of the Alpine orogeny resulted in the development of the Molasse Basin between the Rhône Valley and Austria (Sissingh 1996). The basin is filled by the typical sequence of clastic sedi-ments to a depth of up to 6 km and obtains its largest width of about 150 km in its eastern part (Fig. 1). The EEC itself was partly cov-ered by relatively thin sediments during its Late Precambrian and Phanerozoic evolution, for example in the area of the Baltic Basin, which also encompasses parts of northern Poland and Lithuania (Nikishin *et al.* 1996, Fig. 1).

The Moho has been extensively studied in Central Europe, from the pioneering observations by Mohorovičić (1910) more than a hundred years ago, via the continent-scale cross section along the European Geotraverse (Ansorge *et al.* 1992), to modern Moho depth maps incorporating results from numerous seismic, seismologi-cal and gravity studies (e.g. Ziegler & Dézes 2006; Grad *et al.* 2009), and velocity models of the whole European crust, for ex-

ample EuCRUST-07 (Tesauro *et al.* 2008) and EPcrust (Molinari & Morelli 2011). For an overview of previous work over the last decades, see Grad *et al.* (2009) and references therein.

Recent large-scale seismic experiments provide a major contribu-tion to the mapping of Moho topography in central Europe. Exam-ples are the refraction and wideangle reflection profiles POLON-AISE'97 (Guterch *et al.* 1999), CELEBRATION 2000 (Guterch *et al.* 2003) and SUDETES 2003 (Grad *et al.* 2003b), which also form the backbone of the Moho depth map by Grad *et al.* (2009) in Poland and the Czech Republic, as well as EUROBRIDGE (EU-ROBRIDGE Seismic Working Group 1999; Yliniemi *et al.* 2001) across the EEC between the Baltic Sea and Ukraine. Dense passive experiments have likewise yielded information on the Moho depth for specific regions, for example the BM (Geissler *et al.* 2005; Heuer *et al.* 2006; Geissler *et al.* 2012), by means of RFs. Coverage with passive experiments across central Europe as a whole including the TESZ has so far remained sparse, though. Crustal structure at the transition from Phanerozoic Europe to the EEC across the STZ has been mapped with RFs only along the northern European TOR pro-file between northern Germany and Sweden (Gossler *et al.* 1999; Wilde-Piórko *et al.* 2002; Alinaghi *et al.* 2003) . Teleseismic events were also recorded and analysed at some short-period stations along the active seismic profile POLONAISE'97-P4 in central Europe, but the recording time of only 3 weeks proved insufficient to reliably determine Moho depths with RFs from this data set (Wilde-Piórko *et al.* 1999). Moho depths have been derived from RFs for perma-nent broad-band stations in central Europe, giving an indication of first-order changes, for example beneath the Alps or across the TTZ (Geissler *et al.* 2008). However, the data set available to Geissler *et al.* (2008) is getting sparser towards the east with a limited num-ber of stations in Poland, only two of them east of the TTZ, and only one station in Estonia to cover the Baltic countries.

In this study, we use data of PASSEQ, the densest passive seis-mic network deployed across central Europe yet, to derive a map of the Moho depth across the TESZ from RFs. In addition, we pro-vide images of crustal structure along migrated RF sections, derive information on average crustal v_P/v_S ratios, and map variations in relative amplitudes of the RF Moho phase, as well as sediment thickness below the stations. We find that variations in the above properties can be correlated with tectonic boundaries as well as geodynamic processes. By comparing RF results with the available active data sets and other previous results, we can make inferences about the reliability and accuracy of our data set. Specifically, this is important when interpreting deeper structures for which no inde-pendent active information is available.

2 DATA AND PROCESSING

2.1 Data set

Our data set consists of teleseismic *P*- and *S*-RFs for stations in central and eastern Europe between the Benelux countries to the west and Estonia, western Russia, Belarus and Ukraine to the east (Fig. 2). The main new contribution within this data set is the use of data from the temporary PASSEQ experiment (Wilde-Piórko *et al.* 2008), which was conducted between eastern Germany and Lithua-nia from 2006 to 2008. With 196 stations, roughly a quarter of which featured broad-band sensors, PASSEQ provides the densest cover-age of any passive seismic investigation in this region yet. The main focus of PASSEQ is the detailed imaging of 3-D structure within the upper mantle across the TESZ, for example lithospheric thickness,
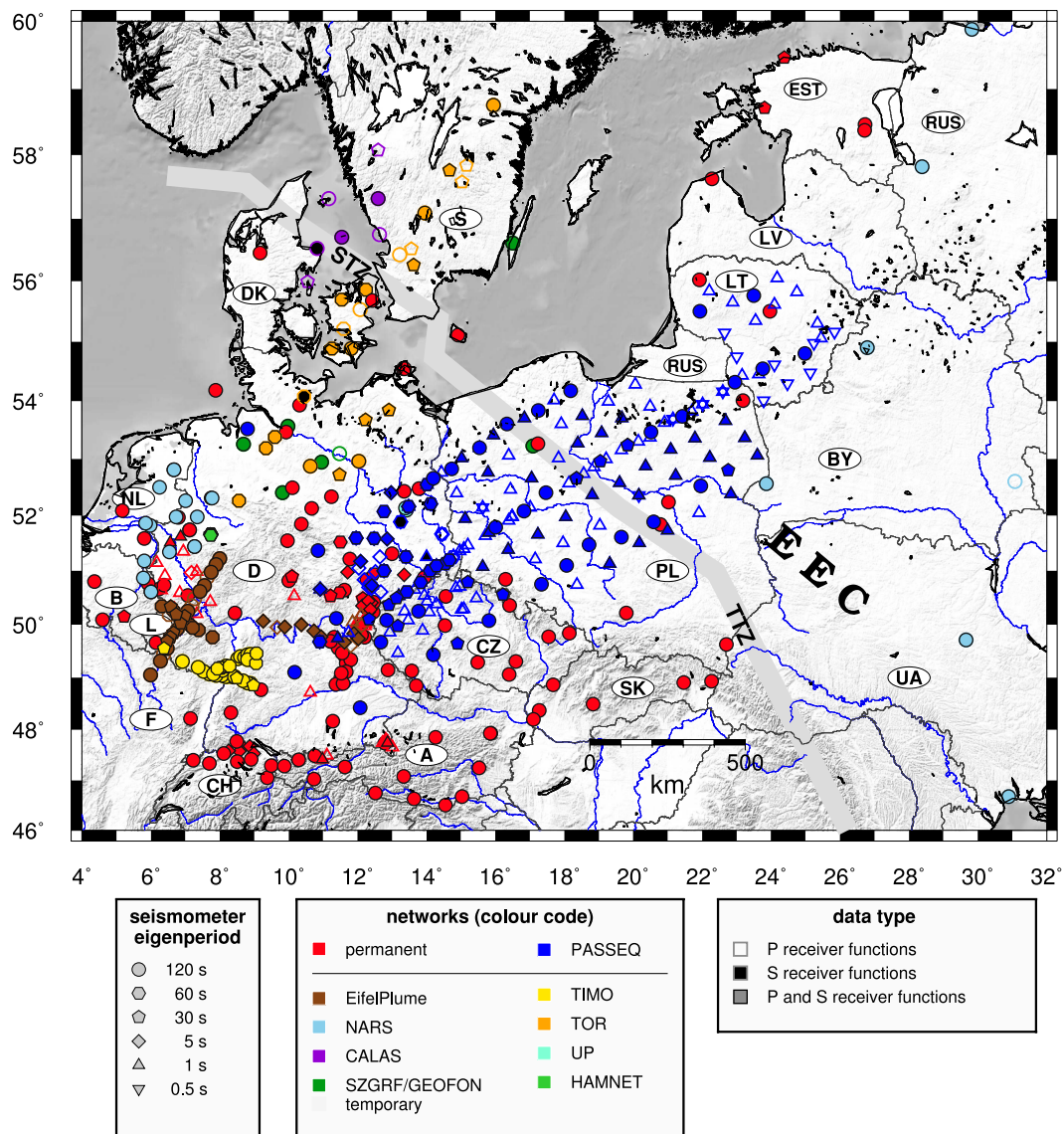
Figure 2. Map of the station distribution used in this study. Different symbol types (lower left inset) mark different instrument types, networks are colour coded (middle inset) and the type of used data is expressed by white infill (only *P*-RF), black infill (only *S*-RFs) or coloured infill (*P*- and *S*-RFs). National boundaries are indicated by dark grey lines and countries labelled. Key to labels: TTZ, Teisseyre-Tornquist Zone; STZ, Sorgenfrei-Tornquist Zone; EEC, East European Craton.

mantle flow (Babuška & Plomerová 2013) and thermal properties of the mantle transition zone (Knapmeyer-Endrun *et al.* 2013). The data set additionally provides valuable information on the Moho topography of the region, which, as explained above, is also relevant to other uses of the data. To complement the PASSEQ data, we used additional data from permanent national and regional networks and broad-band stations from other temporary experiments in the broader region (Paulssen *et al.* 1990; Budweg *et al.* 1999; Gregersen & the TOR Working Group 1999; Paulssen *et al.* 1999; Ritter *et al.* 2008; Medhus *et al.* 2009; Wehling-Benatelli *et al.* 2013), resulting in 495 analysed stations in total (see also Tables S1 and S2).

2.2 *P*-receiver functions

The *P*-RF technique uses *P*-to-S converted phases in the teleseismic *P*-wave coda to derive information on seismic discontinuities, for example the Moho, along the ray path. Since its introduction more than 30 yr ago (Vinnik 1977; Langston 1979), it has become an es-

tablished method for broadband as well as short-period data. We use both *P*- and PKP-phases in our analysis, as the latter can be useful to image dipping structures (e.g. Levin & Park 2000; Knapmeyer & Harjes 2000). We manually selected the data based on the signal-to-noise ratio of the *P*- or PKP-onset from a catalogue of all events with magnitudes of 5.5 or greater at hypocentral distances between 30° and 97° for *P*- or larger than 141° for PKP-RFs, respectively. After restitution of the instrument responses, we rotated the seismograms into the LQT ray coordinate system. The rotation angles were derived by polarization analysis of the first onset (Jurkevics 1988). This approach proved to be problematic for a small number of temporary stations that were located on thick sediments with a strong velocity contrast to the bedrock, for example within the Polish Basin. At these locations, strong reverberations on the horizontal components prevent a sensible measurement of azimuth and incident angles from polarization and the data were instead rotated in the ZRT-coordinate system, using the theoretical azimuth. The ZRT-coordinate system provides reasonable results in these cases as

the slow sediment velocities lead to rather steep incidence angles at the surface. These produce an approximate natural separation between *P*- and *S*-wavefields on vertical and horizontal components. Finally, the L- (or Z-, respectively) component was deconvolved from all three components in the time domain by means of a Wiener filter (Kind *et al.* 1995). All traces were bandpassed between 2 Hz and a variable lower limit before deconvolution. The lower corner frequency of the bandpass filter varied between 10 s and 50 s, primarily related to the sensor bandwidth. We selected RFs with low amplitudes before the *P*-onset and a clear Moho signal for further analysis. This procedure resulted in a data set of 27,468 *P*-RFs from 480 stations.

2.3 *S*-receiver functions

The *S*-RF technique was introduced more recently by Farra & Vinnik (2000) and uses *S*-to-*P* converted phases that occur as precursors to the teleseimic *S*-wave. The clear separation between the direct conversions and multiple converted and reflected phases, which arrive only after the teleseismic *S* wave, allows for the unambiguous imaging of discontinuities within the shallow upper mantle with *S*-RF, while signals from these depths are often masked by multiples in *P*-RFs. Hence, *S*-RFs have contributed significantly to the mapping of the lithosphere-asthenosphere boundary (LAB) across the world (see Artemieva 2011; Kind *et al.* 2012, for recent overviews). While the LAB is often the chief target of *S*-RF studies, we use *S*-RFs here in complement with *P*-RFs to map crustal thickness. The LAB beneath central Europe is the topic of a further, ongoing study.

Due to the lower frequency content of teleseismic *S*- compared to *P* waves, the *S*-RF method is generally applied to broad-band stations (e.g. Li *et al.* 2004; Hansen *et al.* 2007; Heuer *et al.* 2007; Kumar *et al.* 2007; Olsson *et al.* 2007; Geissler *et al.* 2010; Hu *et al.* 2011). Nevertheless, the applicability to short-period sensors (eigenperiod of 5 or 1 s) has also been demonstrated, for example in studies by Sodoudi *et al.* (2006, 2009) and Taghizadeh-Farahmand *et al.* (2010). The majority of the PASSEQ stations was equipped with short-period sensors, so naturally we tried to apply the *S*-RFs method to these. However, for a significant amount of the stations, we were not successful in obtaining *S*-RFs (compare open blue triangles in Fig. 2), either because the number of potentially usable events recorded was too small or because we could not identify any clear S-onsets, neither in the restituted nor in the raw data. This might be related to the type of sensor used, and the type and settings of the digitizer. The PASSEQ data set is quite heterogeneous in this respect, with five different short-period sensors and six types of data loggers with changing gain settings used in various combinations. We managed to obtain reasonable *S*-RFs for some of the short-period stations, also from other networks (Lennartz 5 s stations of the Swiss Seismological Service's network and Saxonian Seismic Network, Marks L4-3D 1 s stations of the Bavarian Network and RuhrNet—for an example, see Fig. 3f).

Based on the theoretical study by Yuan *et al.* (2006), we consider *S*-phases for events of magnitude greater than 5.7 at epicentral distances between 60° and 80° and *SKS*-phases for events of magnitude greater than 5.8 at epicentral distances between 85° and 120°. We rotated the traces into the ray coordinate system using theoretical azimuth and incidence angles after checking (and correcting for) possible misorientations of the station. Azimuthal deviations of more than about 10° and especially polarity or component switches of the horizontal components show up clearly when comparing theoretical and measured azimuths from the previous analysis of *P*-RFs.
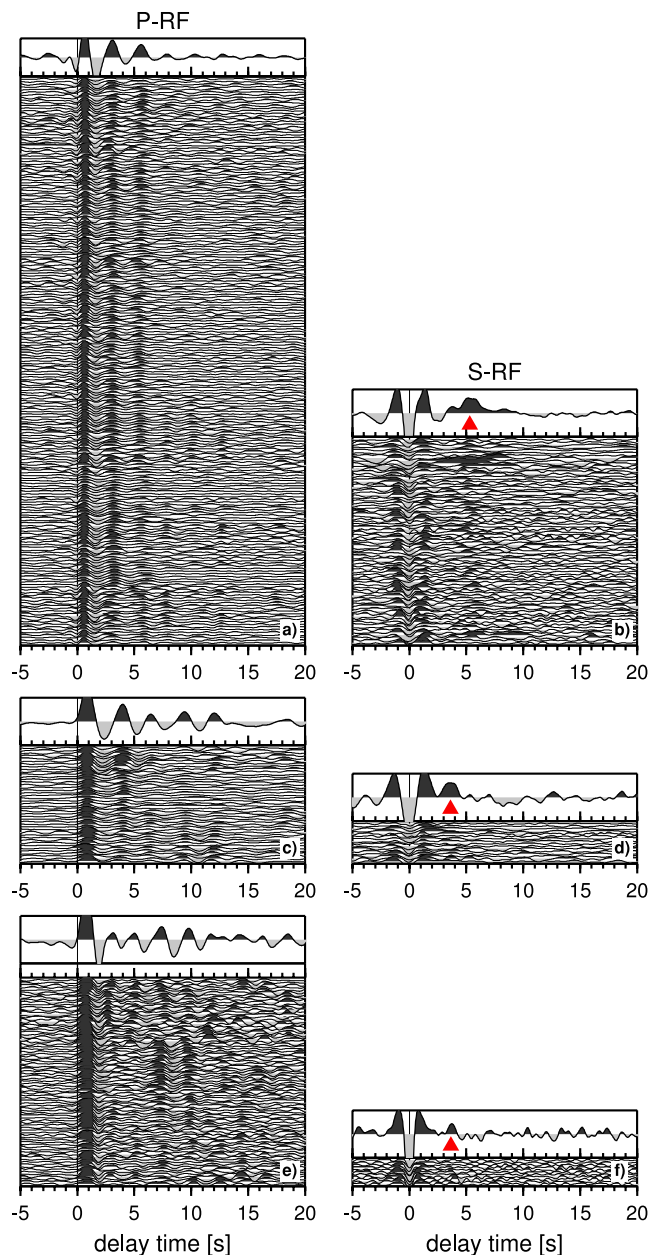

Figure 3. Examples of *P*- and *S*-RFs at stations that show a strong sediment effect. All individual RFs are filtered with a low-pass at 1 s, move-out corrected to a slowness of 6.4 s deg^{-1} and sorted by backazimuth, with the sum trace at the top. The Moho conversions in the *S*-RFs are indicated by red triangles. (a) Permanent broad-band station SUW in eastern Poland, 213 *P*-RF, (b) Station SUW, 78 *S*-RFs, (c) Temporary broad-band PASSEQ-station PA64 in western Poland, 44 *P*-RF, (d) Station PA64, 16 *S*-RFs, (e) RuhrNet short-period station BRHE in western Germany, 84 *P*-RF (f) Station BRHE, 11 *S*-RFs.

We then deconvolved the Q-component from all three components, again using a Wiener filter in the time domain. To make the resulting *S*-RFs comparable to their *P*-counterparts, we reversed the time axis and the polarity of the traces. The use of theoretical angles can lead to large negative arrivals with significant side lobes around zero time in the case of a surficial low-velocity layer (Fig. 3). Nevertheless, the Sp conversion from the Moho is always clearly recognizable. We automatically removed the most noisy and unreliable data by selecting only traces with a minimum peak amplitude of 0.08

relative to direct S within the time window ± 1.5 s around the Moho onset time of the *P*-RFs at the same station and root-mean squared relative amplitudes of less than 0.1 averaged over the time window between 10 and 40 s. For 33 stations, mainly in the cratonic area of the study region, which showed broad Moho conversions of smaller amplitudes, the minimum peak level was lowered to 0.07 relative to direct S. This left us with 14 399 *S*-RFs from 332 stations.

2.4 Estimation of Moho depth

An initial estimate of the Moho depth can be obtained from the delay time of the corresponding Ps or Sp conversion. To measure the delay times, the RFs were move-out corrected to a common slowness of 6.4 s deg^{-1} and stacked. *P*-RFs generally sample the Moho at distances of less than 20 km from the recording station, even for large Moho depths exceeding 40 km, as expected beneath the EEC. *S*-RFs, however, sample the Moho at significantly larger distances from the station, which might exceed 50 km. The Sp piercing points show little overlap with the area sampled by *P*-RFs at the same station, but might overlap between different stations as, for example, the average interstation distance of PASSEQ is 60 km. Thus, we stack *P*-RF by station, but *S*-RFs are binned and stacked according to piercing points at Moho depth on a roughly 20 km-grid (0.18° latitude by 0.29° longitude). 20 km is the order of the estimated Fresnel zone radius for *S*-RFs at Moho depth in Phanerozoic Europe; within the EEC, the estimate of the Fresnel zone radius is on the order of 30 km due to the larger crustal thickness and higher lower crustal velocities. Only stacks with at least 5 traces are used in both cases; stations and bins with less data were discarded. To calculate the Sp piercing points at Moho depth, however, a first estimate of this depth is needed for each station. To obtain this estimate, we used the Moho depth map by Grad *et al.* (2009), which is based on a large number of data sets mainly from seismics, but also including gravity, RFs and surface wave data. We interpolated the map to the station locations, with the resulting depth values rounded to 0.5 km accuracy. Piercing points are calculated by tracing each ray backwards from the surface to the Moho depth interpolated for the corresponding station, using velocities from the standard 1-D Earth model *iasp91* (Kennett *et al.* 1995). This model does surely not provide the true crustal structure for the EEC. However, comparing piercing points calculated with velocities from *iasp91* and from a more realistic crustal model based on Grad *et al.* (2003a) for selected stations on the EEC shows that deviations in piercing point locations are generally small for *P*-RF, that is below 500 m, and can safely be ignored. For *S*-RFs, which have a longer travel path through the crust due to their shallower incidence angle, piercing point locations might differ by as much as 10 km for crustal thicknesses approaching 50 km, shifting locations closer to the station. Still, for the majority of waveforms used on the EEC, differences are smaller than 5 km and are neglected here.

For stations located on slow sediments with a strong velocity contrast to the layer below, *P*-RF tend to be dominated by reverberations within the sediment layer that arrive in regular intervals and can mask the Moho conversion (Fig. 3). In these cases, the clear separation between direct Sp conversions and their multiples on different sides of the *S*-wave arrival in *S*-RFs can guide the selection of the correct Moho peak in the *P*-RF, or, in cases where no corresponding peak is found in the *P*-RF (e.g. station BRHE, Figs 3e and f), lead to the rejection of the *P*-data set. The delay times of the Moho onsets and their standard deviations were determined by bootstrapping with full replacement over 100 000 samples (Efron

& Gong 1983). Only stations with standard deviations of less than 0.2 s and bins with standard deviations of less than 0.4 s are shown in Fig. 4. The limit chosen for the *S*-RFs is wider due to their lower frequency content which leads to a larger uncertainty in the timing of the amplitude peak. In addition to providing delay times, the colour scale in Fig. 4 is translated to pseudo depths by using an average crustal *P*-wave velocity of 6.2 km s^{-1} and a constant v_P/v_S ratio of 1.73.

Although the delay time picks give a first-order impression of Moho depth variations within the covered region, estimates can be improved by considering variable crustal *P*- and *S*-wave velocities. Specifically, sedimentary basins can cause significant delays in arrival times that can be accounted for by using accurate crustal velocities (Yeck *et al.* 2012). To determine Moho depths, we applied the method of Zhu & Kanamori (2000), which makes use of the distinct move-out behaviour of direct conversions and multiples to constrain the depth to a discontinuity and the average v_P/v_S ratio above. Given an average crustal *P*-wave velocity, weighted *P*-RF amplitudes are stacked along theoretical move-out curves calculated on a grid of depth versus v_P/v_S values for both the direct Ps-phase and the PpPs- and PsPs/PpSS-multiples. For the true depth and v_P/v_S ratio, the three phases should sum constructively and thus result in an amplitude maximum in the stack matrix (Fig. 5). The weights assigned to the different phases are 0.5, 0.3 and 0.2, respectively. Besides, we calculated the coherence between the three different phases over a time window of 3 s around the theoretical onset times when stacking the data and used their semblance as an additional weighting factor (Chen *et al.* 2010). This type of semblance weighting significantly reduces the trade-off between depth and v_P/v_S ratio and leads to more unambiguous results (Kieling *et al.* 2011; Tkalčić *et al.* 2011). We did not use the individual recorded traces as input to the Zhu & Kanamori (2000) stacking, but first binned and summed them in bins of 0.1 s deg^{-1} width with 50 per cent overlap. The complementary use of data with a number of different ray parameters is essential to capture the move-out behaviour of the different phases in the stacking. The initial summation should prevent the predominance of a single strong source region, that is a single very limited ray parameter range, characterized by a high number of usable earthquakes, over the final stacks.

Grad & Tiira (2012) have shown that the use of global velocity models instead of adequate information on regional crustal velocity structure can result in biases of up to 5 km when estimating Moho depths from RFs. Hence, we used the most detailed and up-to-date information on average crustal *P*-wave velocities available when applying the method of Zhu & Kanamori (2000) to our data. In detail, average velocities were calculated from Majdański (2012) for Poland, from Karousová *et al.* (2012) for the Czech Republic and from EPcrust (Molinari & Morelli 2011) for the rest of the covered area.

In addition to the application to *P*-RF, we also used the Zhu & Kanamori (2000) method for *S*-RFs (Wittlinger *et al.* 2009). Unlike Wittlinger *et al.* (2009), we did not invert *P*- and *S*-RFs jointly by station, though, as they do not sample the same area. For *S*-RFs, the significant multiple phases are SsPp/SpSp and SsSp. In contrast to the Ps case, the first multiple phase has the opposite sign of the direct conversion, and the second multiple phase has the same sign as the direct conversion. Multiples are less clear to identify in the Sp case (Fig. 6), which might be due to a inherently lower frequency content or the fact that they sample the Moho over an even broader distance range than the direct conversion. Only bins with clearly identifiable maxima were used in the further analysis. Processing is similar to that for *P*-RF described above, except that an average crustal *S*-wave
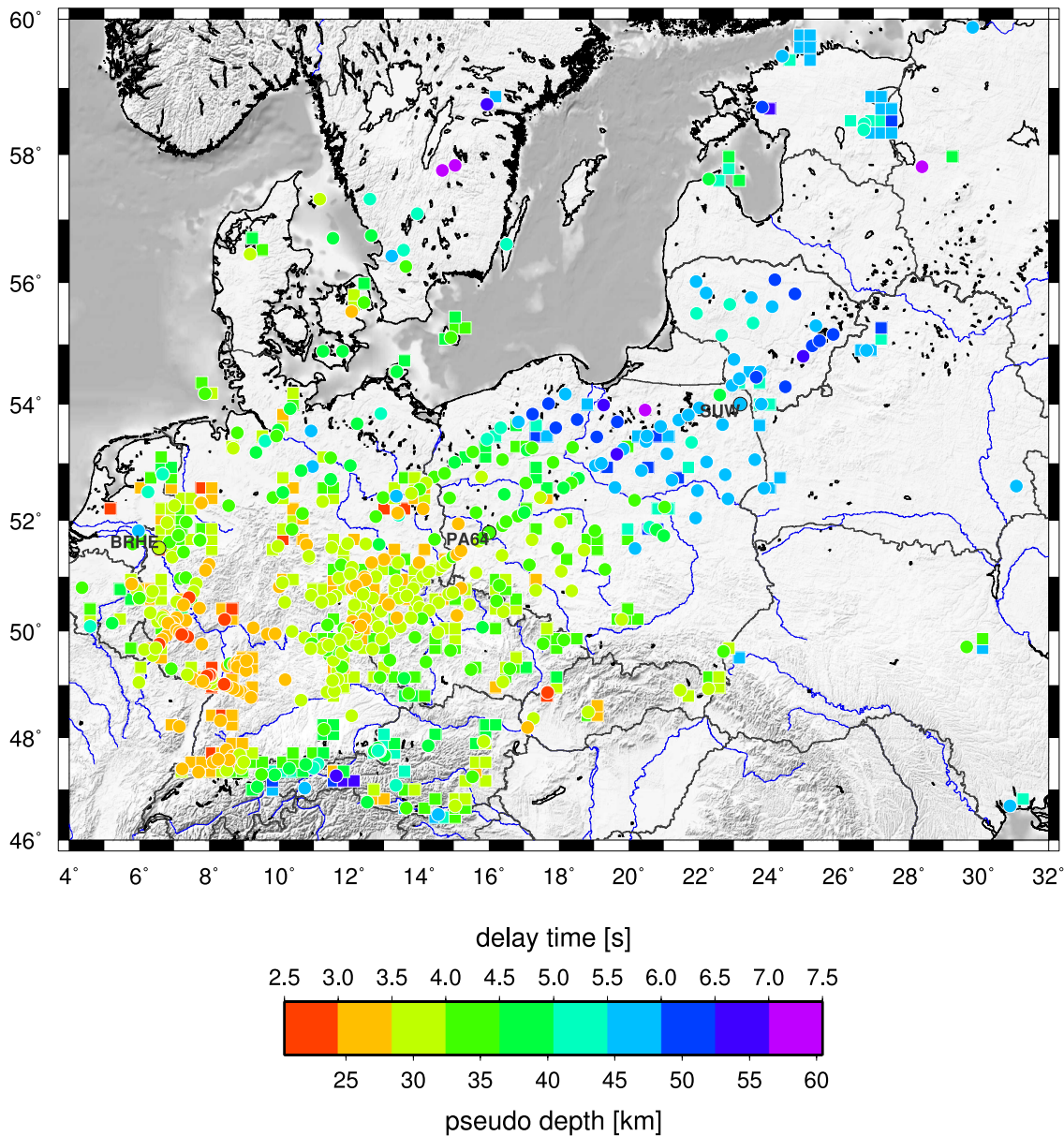
Figure 4. Map of measured delay times of Ps and Sp conversions from the Moho. Circles mark station locations for Ps measurements, whereas boxes mark bins used in Sp measurements. Pseudo Moho depth is computed using an average crustal *P*-wave velocity of 6.2 km s^{-1} and a constant v_P/v_S ratio of 1.73. Stations for which data is shown in Fig. 3 are marked by black circles and labelled.

velocity is needed instead of a *P*-wave velocity. These *S*-wave velocities were calculated from EPcrust (Molinari & Morelli 2011), as the other, more detailed models give only *P*-wave velocities.

To determine the uncertainty in the derived values for Moho depth and v_P/v_S ratio, bootstrapping with full replacement and 7500 samples was performed on the Zhu & Kanamori (2000) analysis for both *P*- and *S*-RFs. To speed up computing, we did not use the full parameter space as shown in Figs 5 and 6 for bootstrapping, but only a limited range of ±8 km around the Moho depth resulting from the initial solution and ±0.18 around the corresponding v_P/v_S ratio. For 30 stations, the parameter range was constrained more to prevent jumping to a completely different maximum. Bootstrapping might not capture the full uncertainty within the RF results, for example caused by the finite Fresnel volume size or uncertainty in the used average crustal velocity, thus leading to rather optimistic error estimates, for example when compared to other data types

(Grad & Tiira 2012; Spada *et al.* 2013). Still, it provides us with consistent estimates for the whole data set that allow for deselection of certain data points based on their relatively larger uncertainty. We obtained estimates of Moho depth and v_P/v_S ratio for 455 stations and 424 bins. In the following, we only used Moho depth estimates with standard deviations below 7.5 per cent, leaving about 80 per cent of the original stations and 70 per cent of the original bins after this selection. All resulting Moho depths as well as Ps and Sp delay times can be found in Tables S1 and S2.

2.5 Migration

Data were migrated by converting traveltime to depth and backprojecting the traces along their ray paths using *iasp91* (Kennett *et al.* 1995). Amplitudes were stacked on a grid with 15 km horizontal
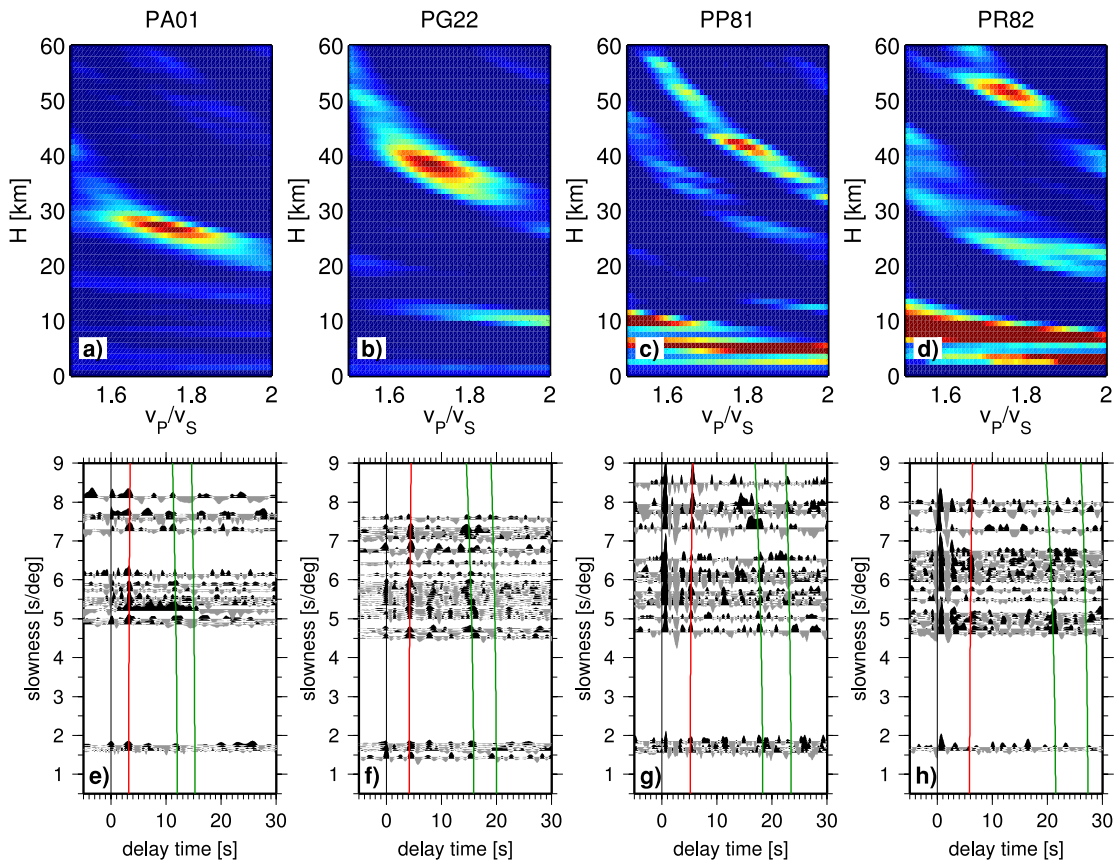
Figure 5. Examples of applying the Zhu & Kanamori ([2000](#)) method to *P*-RF. Shown are coherency-weighted stacks and slowness sections of RFs for four different temporary PASSEQ stations, from west to east (see Fig. [7](#)a) for locations). Coloured lines in the slowness sections indicate theoretical arrival times for the direct Ps conversion (red) and the first two multiples (green) calculated for the best Moho depth and v_P/v_S ratio as determined from bootstrapping of the stacks. (a) and (e) Broad-band station PA01, average crustal *P*-wave velocity $\overline{v_P}$ used in the analysis is 6.02 km s^{-1}, (b) and (f) Broad-band station PG22, $\overline{v_P} = 6.47$ km s^{-1}, (c) and (g) Short-period station PP81, $\overline{v_P} = 6.28$ km s^{-1} (d) and (h) Short-period station PR82, $\overline{v_P} = 6.53$ km s^{-1}.

and 2 km vertical spacing. Waveform amplitudes were attributed to all bins within 25 km of the piercing point at the corresponding depth level, with weighting linearly reduced to zero for distances between 12 and 25 km. This corresponds to full weighting within the first Fresnel zone of the Ps-phases at 35 km Moho depth, and smoothly degrading influence outside of that zone. For the profile sections, grid cells within ±35 km distance from the profile lines were projected on the profiles in bins of 20 km width. The same procedure was applied to both *P*- and *S*-RFs and also to the *P*-multiples, PpPs and PpSs + PsPs. Due to the greater compression of the time axis when mapping the traveltimes of multiples to depth, signals appear sharper in the images of migrated multiple phases, even though the data were low-passed at 3 s before migration of the multiples. The multiples can sample regions at greater distance from the receiver than the primary conversions and should be devoid of spurious signals at upper mantle depth that result from the constructive stacking of multiples in the migration of *P*-RFs. However, incorrectly projected direct Moho phases tend to contaminate the images reconstructed from multiples at shallow crustal depths.

3 RESULTS

3.1 Moho depth

The delay time map of the Moho phase shows some distinct and well-known trends (Fig. [4](#)). The average delay time in the central

part of the region, around the German–Polish–Czech boundary, is about 3.9 s. Significant deviations are found in tectonically active areas, that is reduced delay times, as low as 2.5 s, in the upper Rhine Graben, and increased delay times of up to 6.9 s beneath the Alps, but also towards the EEC. Whereas delay times around 4.5 s are observed in Poland west of the TTZ and in Denmark, the surface trace of the STZ–TTZ is co-located with an increase in delay times to more than 5.5 s. Maximum delay times within the EEC reach 7.4 s, but the distribution shows some local variations, for example an increase in delay times from northwestern to southeastern Lithuania.

A similar picture emerges from the Moho depth estimates (Zhu & Kanamori [2000](#)). Here, the STZ–TTZ roughly coincides with the 40 km depth contour of the Moho in both Poland and Scandinavia (Fig. [7](#)). A further increase in depth to more than 45 km is found more than 200 km to the northeast near the Lithuanian border. Locally, for example beneath southern Sweden and in eastern Lithuania, Moho depths in excess of 50 km are reached, whereas measurements at two isolated locations in southern Ukraine point to a shallower Moho around 40 km in this region. The shallowest Moho, at a depth of less than 25 km, is found in the upper Rhine Graben. A local minimum with depths around 27 km also marks the Eifel region west of the main Rhine Graben structure around 7°E, 50.5°N. As coverage is rather dense in this area (Figs [2](#) and [7](#)a), we consider this result reliable. Measurements in Slovakia south of the Carpathian arc likewise indicate a Moho depth of less than 25 km within the Pannonian Basin. Another distinct local anomaly is the transition to larger Moho depths (>35 km) in the south-western (Moldanubian)
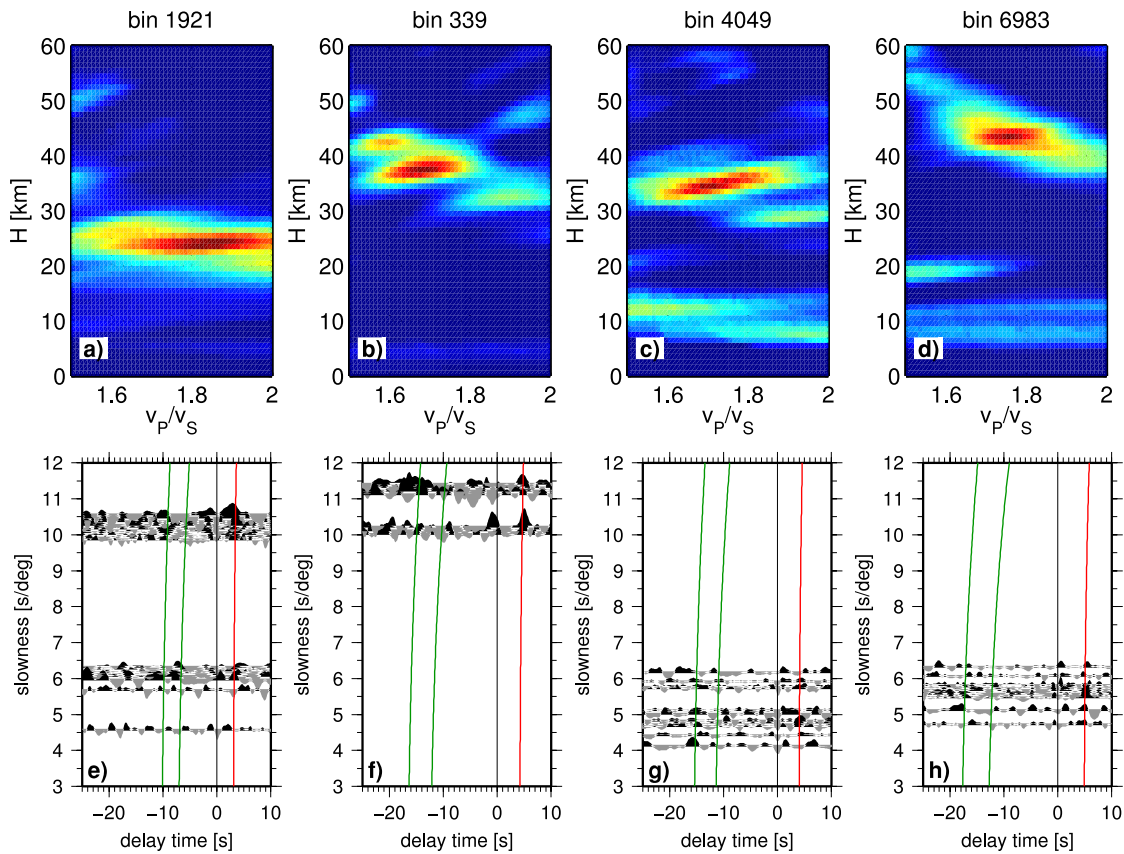
Figure 6. Same as Fig. 5, except for *S*-RFs. Data are not considered station-wise, but bin-wise in this case (see Fig. 7a) for locations). (a) and (e) Bin 1921, average crustal *S*-wave velocity $\overline{v_S}$ used in the analysis is 3.47 km s^{-1} (b) and (f) Bin 339, $\overline{v_S} = 3.58$ km s^{-1} (c) and (g) Bin 4049, $\overline{v_S} = 3.50$ km s^{-1} (d) and (h) Bin 6983, $\overline{v_S} = 3.80$ km s^{-1}.

part of the BM. Beneath the northern Alps, Moho depth increases up to 55 km in southern Austria. The strong gradient in crustal thickness is also nicely imaged across northern Switzerland, from Moho depth around 27 km in the Rhine Graben in the west, to Moho depth around 40 km beneath the Alpine arc in the east. In general, the Moho topography looks more gradual and less sharp across the TESZ compared to the more recently active Alpine region.

3.2 Crustal sections along migrated profiles

RFs were migrated along four profiles (Fig. 7b). Profiles A–A′ and C–C′ are roughly perpendicular to the strike of the TTZ and cover the northern and southern extend of the PASSEQ data set. East of the German–Polish border, profile A–A′ is also identical to the seismic profile P4 of POLONAISE'97 (Grad *et al.* 2003a). Profile B–B′ extends across the covered part of the EEC from southern Scandinavia to eastern Lithuania, whereas profile D–D′ is located within Phanerozoic Europe and extends from the Dutch coast to the Austrian Alps. Along all profiles, migrated slices through the *P*-RF were calculated for the direct conversions (parts (a) and (f) of Figs 8 and 9) as well as for the multiples. The latter were summed, after correcting for the sign of the second multiple, to create parts (b) and (g) of the figures. For the direct conversions, erroneously projected multiples are clearly seen, especially in the western halves of profiles A–A′ and C–C′, at depth between 100 and 150 km, whereas in the migration of multiples, the direct conversions map into the shallow crust and should not be interpreted in terms of structure. Besides, the graphical output of the method of Zhu & Kanamori (2000) for the optimum v_P/v_S ratio was projected on the profile line for stations

within ±50 km (parts (c) and (h) of the figures). Finally, *S*-RFs were also migrated along the profiles (parts (d) and (i)), and we display the results of the method of Zhu & Kanamori (2000) for the Sp data set along the profiles in parts (e) and (j).

Along profiles A–A′ and C–C′, the change in crustal thickness across the TESZ is readily apparent, from Moho depths of around 30 km to the west to depth of around 50 km to the east. This drop occurs over about 200 km laterally in both cases. Whereas the changes seem to occur as a stepwise transition when looking at the direct conversions (Figs 8a and 9a), they look more gradual when imaged by the multiples (Figs 8b and 9b). In both cases, Moho and crustal structure is complex across the TESZ. Along both profiles, a prominent negative (blue) conversion is imaged at shallow depth beneath the craton and dips towards the Moho east of the TTZ. Whereas a similar feature is found at the eastern end of profile B–B′ (Fig. 8f), inclined towards the Baltic Sea, this structure is neither found in the images of the migrated multiples, nor in the *SP*-RF. As discussed below (Section 4.5), it is most likely an artefact caused by erroneous projection of multiples from a low-velocity surficial sediment layer. Within Phanerozoic Europe, shallow Moho depths around 24 km are found for both direct Ps conversions and multiples when crossing the Rhine graben (between 8.5°E and 10.4°E on profile A–A′, and more localized, around 9.5°E on profile C–C′, Figs 8a and b, and 9a and b). The corresponding Moho uplift is also found along the perpendicular profile D–D′ at around 50.75°N (Figs 9f and g). The most prominent feature along D–D′ is imaged at its southern end, though, where the Moho drops to 50–55 km depth beneath the Alps. This drop is marked by a rather abrupt step at about 47.6°N (Figs 9f and g). Moho topography along profile B–B′ within the
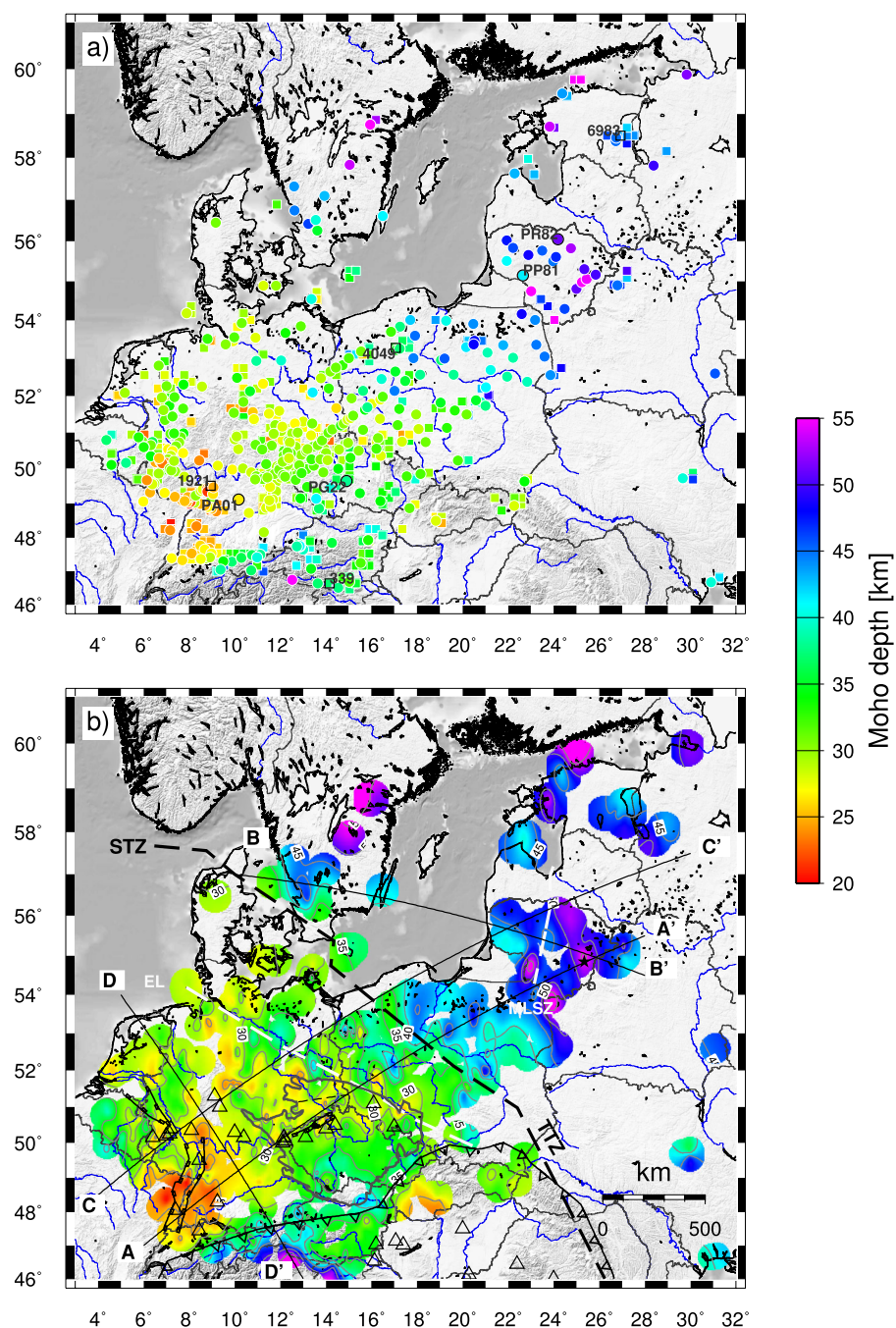
Figure 7. Moho depth results. (a) Colour coded Moho depth at each station (circles) or bin (boxes) determined by the method of Zhu & Kanamori (2000). Stations and bins used as examples in Fig. 5 and 6 are outlined in black and labelled. (b) Interpolated Moho depth map based on the data shown in (a). Triangles mark Cenozoic anorogenic alkaline volcanoes (Legendre *et al.* 2012). The STZ–TTZ, Alpine-Carpathian front, graben systems and the BM (outline after Plomerová *et al.* 2005) are indicated. Dashed white lines give the location of the Elbe Line EL (Pharaoh *et al.* 2006) and of the Middle Lithuanian Suture Zone MLSZ (Kozlovskaya *et al.* 2001). Profiles used for RF migration in Figs 8 and 9 are denoted by solid black arcs. Thin dashed black line denotes the SW end of POLONAISE profile P4 (Grad *et al.* 2003a), which is identical to A–A′ east of a kink at the German-Polish border up to its NE end point in Lithuania marked by a black star.

EEC is more subdued. The Moho is imaged at an average depth of 47 km within Lithuania, with a localized 5 km-drop around 25.3°E, and lies about 5 km shallower at the edge of the craton within southern Scandinavia (Figs 8f and g). All along the profiles, a positive conversion from very shallow depth seems to point to a thin sediment cover or weathering layer. Indications for further intracrustal structure, apart from the described dipping layer within the craton, are absent.

The Zhu & Kanamori (2000) results for *P*-RF indicate a more complex structure west of the TTZ, between about 15.7°E to 18.4°E, below the Polish Basin (Fig. 8c). A continuous shallower structure is imaged at about 10 km depth beneath Phanerozoic Europe (Figs 8c and e, 9c, e, h and j). There are also indications of a discontinuity between 15 and 20 km depth beneath the craton (Figs 8c and h, 9c). There is a caveat when looking at shallower structure on these plots, though. One has to keep in mind that average velocities across
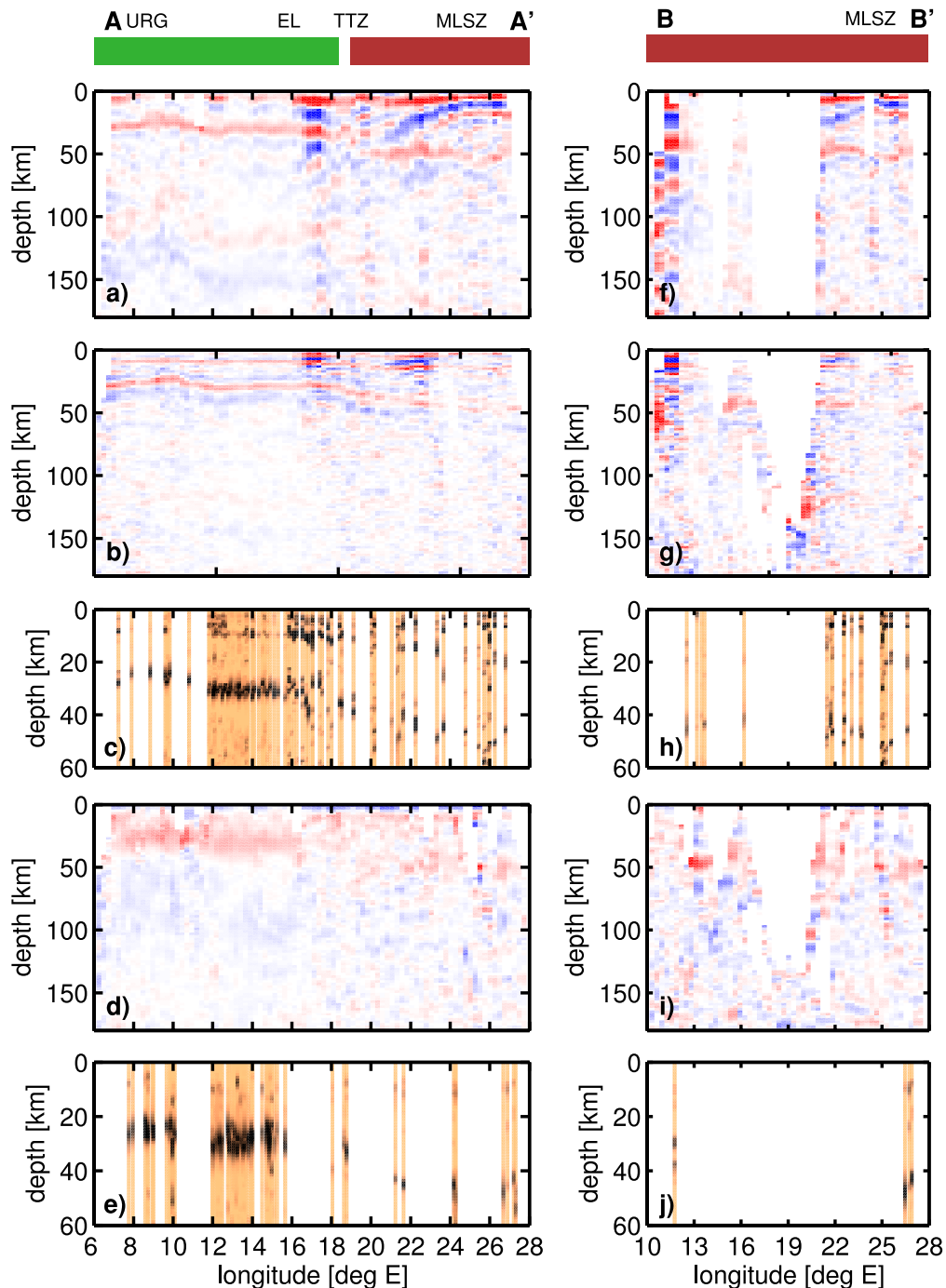
Figure 8. RF sections along southern profile A–A′ (a–e) and eastern profile B–B′ (f–j): Bar on top provides tectonic information along profiles: green for Phanerozoic Europe, red for EEC; EL, Elbe Line; MLSZ, Mid-Lithuanian Suture Zone; TTZ, Teisseyre-Tornquist Zone; URG, Upper Rhine Graben. (a) and (f) Migrated *P*-RF, (b) and (g) summation of migrated PpPs and PpSs multiples, (c) and (h) results from method of Zhu & Kanamori (2000) applied to *P*-RF along profiles, (d) and (i) migrated *S*-RFs, (e) and (j) results from method of Zhu & Kanamori (2000) applied to *S*-RFs along profiles. Profile lines are defined in Fig. 7. Note the difference in depth scale for panels a, b, d, f, g, i and panels c, h, e, j.

the whole crust were used in their computation. For intracrustal structures, lower stacking velocities would be appropriate, which affect the depth attributed to these structures, that is raise them to shallower levels. Thus, the high amplitudes at intracrustal depths in the Zhu & Kanamori (2000) plots in Figs 8 and 9 should only be taken as indication of additional intracrustal structure, without actually interpreting absolute depth values.

3.3 Poisson's ratio *ν*

The method of Zhu & Kanamori (2000) provides not only information on Moho depths, but also on average crustal v_P/v_S ratios. These, in turn, can be used to calculate crustal Poisson's ratios *ν* for the stations considered. Crustal Poisson's ratios are of special interest as they are more sensitive to rock composition than, for
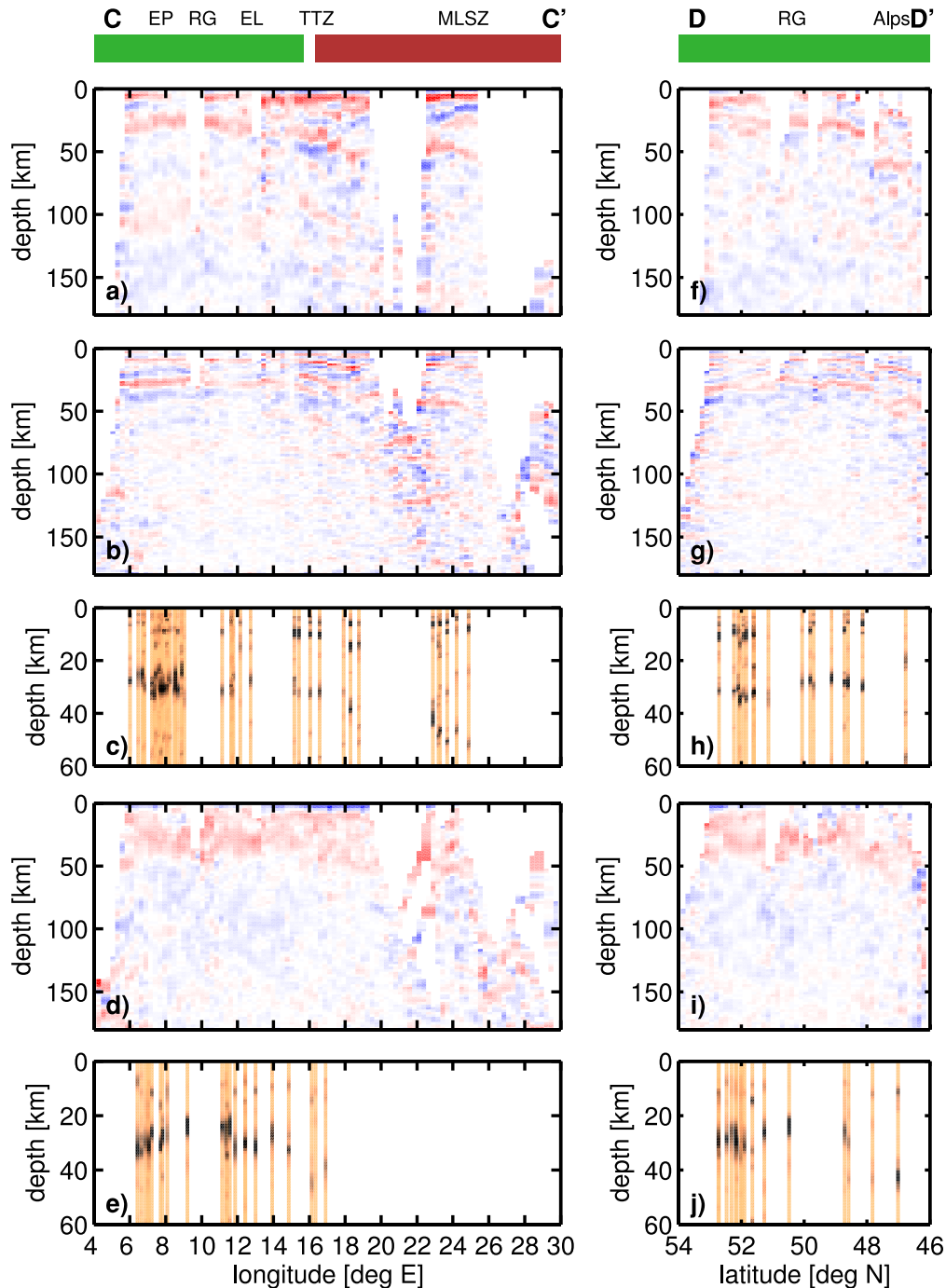
Figure 9. Same as Fig. 8 for northern profile C–C′ (a–e) and western profile D–D′ (f–j). Profile lines are defined in Fig. 7. EP, Eifel Plume; RG, Rhine Graben. Note the difference in depth scale for panels a, b, d, f, g, i and panels c, h, e, j.

example, *P*-wave velocities. Specifically, Christensen (1996) report a linear relation between increasing ν and decreasing SiO_2 content for magmatic and metamorphic rocks, which can be used to distinguish between a more felsic and more mafic lithology. In sedimentary rocks, cracks and pore space have a significant effect on ν (Tatham 1982), resulting in very high values that have for example been observed in porous and water-saturated rocks (White *et al.* 1992, $\nu = 0.3$–0.4) or unconsolidated marine sediments (Hamilton 1979, $\nu = 0.4$–0.49).

Typical results from RF analysis by the method of Zhu & Kanamori (2000) cover a larger range in v_P/v_S space than in terms of Moho depth, though, due to the shape of the various phases' move-out curves (e.g. Figs 5a and 6c). Besides, v_P/v_S values might sometimes be unrealistically high or low due to, for example, interference with intracrustal phases, or Moho topography that causes direct phases and multiples to sample different structures (Zandt *et al.* 1995). Accordingly, we applied a rather conservative selection to the data, in using only data points with standard deviations
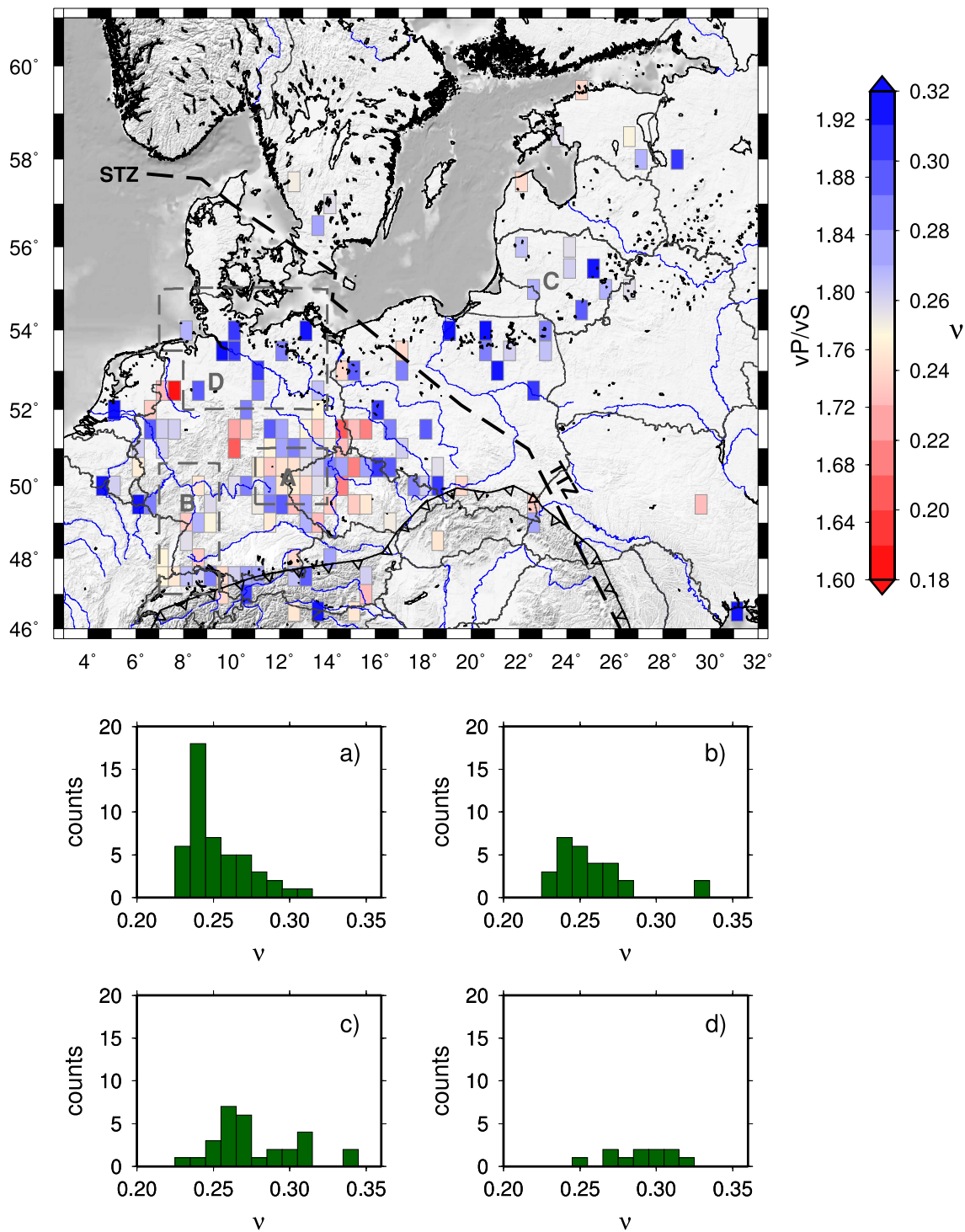
Figure 10. Best determined Poisson's ratios ν (standard deviations from bootstrapping below 0.01) averaged on a $0.5° \times 0.5°$ grid. Histograms show comparison between all individual measurements within different regions outlined by grey dashed lines on map: (a) north-western Bohemian Massif (Saxo-Thuringian and Tepla-Barrandian units), (b) Upper Rhine Graben, (c) EEC, (d) northern Germany.

from bootstrapping that lie below 0.01 in ν. This selection of the best constrained data is also necessary as the variations in average ν that can be expected from crustal lithology are in the range of 0.02 (Zandt & Ammon 1995). The selected high-quality data set is displayed in Fig. 10, averaged on a $0.5° \times 0.5°$ grid. Still, extremely high or low values for ν of less than 0.18 or more than 0.32 are found at some isolated spots. However, several tendencies with regard to the different tectonic units can be observed: Within the EEC (region

C in Fig. 10), we find higher ν than in the densely covered centre of our study region along the Czech–German border (region A) or along the southern Rhine Graben (region B). High ν, with an average value of 0.29, is also detected within the North German Basin (region D). Whereas about 10 per cent of all values are below 0.25 in regions C and D, more than 50 per cent of all samples lie below 0.25 in regions A and B. Median values of ν are 0.25 in regions A and B, 0.27 in region C and 0.29 in region D. A Kolmogrov-Smirnov
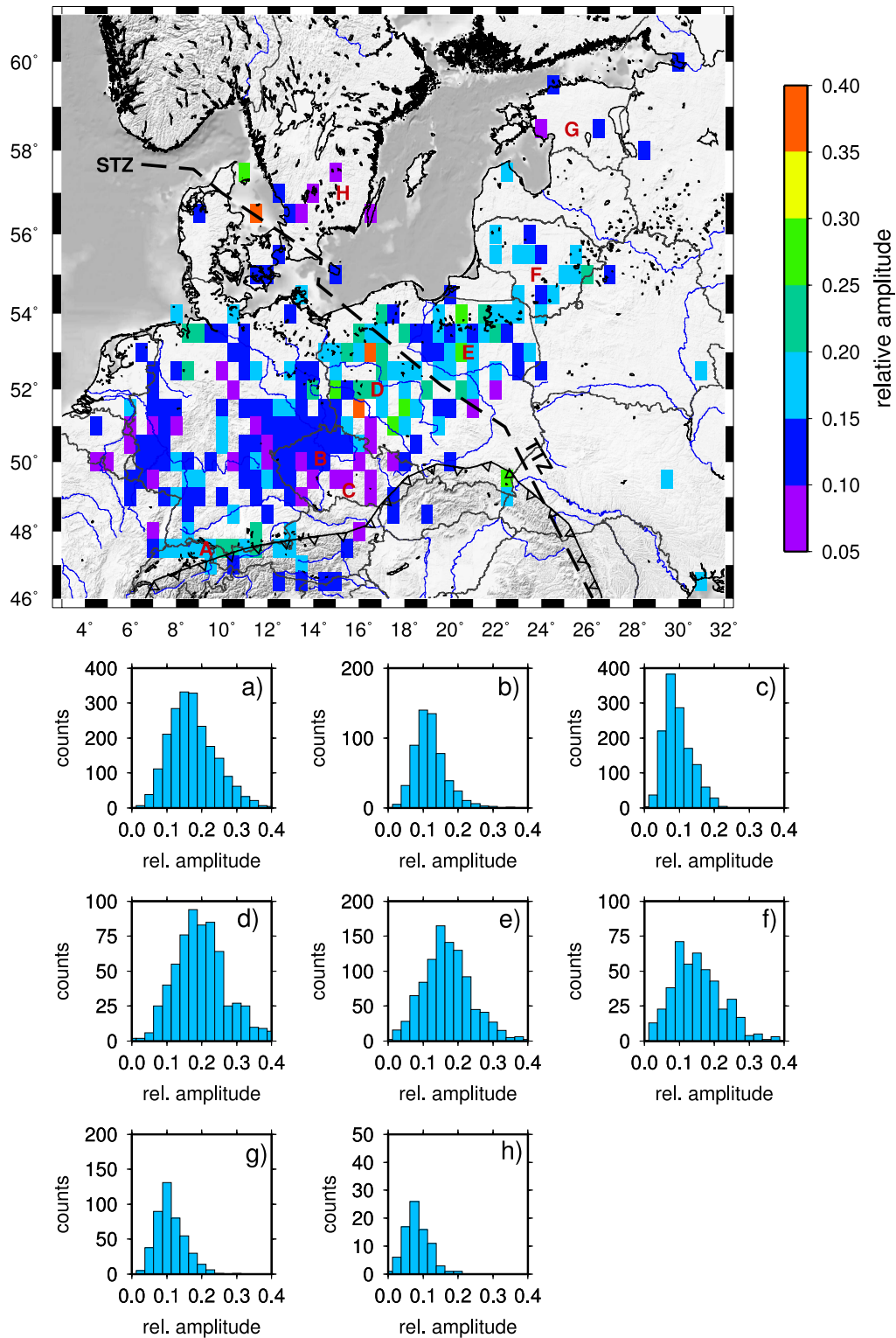
Figure 11. Variations in relative amplitude of the Ps conversions from the Moho (see text for data selection). Histograms are calculated over distinct regions: (a) northern Alpine foreland, (b) Tepla-Barrandian of Bohemian Massif, (c) Moldanubian of Bohemian Massif, (d) Polish Basin, (e) Poland east of TTZ, (f) Lithuania, (g) Estonia, (h) Sweden.

test (Press *et al.* 1992a) indicates that the measured distributions of v are significantly different between the north-western BM and the Upper Rhine Graben on the one hand, and the EEC and northern Germany on the other hand, with a confidence level of 3 per cent.

3.4 Moho phase amplitudes

The amplitude of the Moho phase in RFs is related to the impedance contrast, and especially the change in v_S, across the Moho. Thus, it can in principle provide additional information on lithology. However, amplitudes also depend on the ray-parameter distribution of

the used events, sharpness of the discontinuity, that is are reduced for gradients, and the interference with reverberations from surficial sedimentary layers. The interpretation may thus not be straightforward and is seldom attempted outside of modelling or inversion. Here, we average amplitudes stationwise, and as the event distributions are similar at the various stations, we assume that any amplitude variations solely due to ray-parameter will average out in the displayed results.

In Fig. 11, we map amplitude variations of *P*-RF. Only *P*-phases are used, as amplitudes of PKP-phases are significantly reduced for horizontal layers. Maximum amplitudes are determined on each trace without move-out correction within ±1 s around the picked Moho onset for the corresponding station. Then, all values that differ by more than 0.5 s from the average timing of the maximum amplitude are discarded. Average values for all stations with at least five amplitude measurements and with a standard deviation of less than 50 per cent of the average are plotted on a 0.5° × 0.5° grid. Some distinct regional variations are obvious. Relatively high amplitudes are found in the Northern Alpine Foreland (Molasse Basin, region A) and the Polish Basin (region D). Furthermore, within the BM we observe a change from low amplitudes in the southeastern (Moldanubian) part (region C) to higher amplitudes in the north-central (Tepla-Barrandian) part (region B). From the Polish Basin eastward, amplitudes decrease from eastern Poland (region E) via Lithuania (region F) to Estonia (region G). Amplitudes on the Scandinavian part of the EEC, in Sweden (region H), are even smaller. Distributions of all regions are different at the 1 per cent confidence level according to a Kolmogorov-Smirnov test.

4 DISCUSSION

4.1 Comparison to previous RF studies

Our results can directly be compared to those published by Geissler *et al.* (2008), which were obtained by the same methods for a more limited number of permanent broad-band stations across central Europe. In total, 64 stations were analysed in both studies with *P*-RF. Besides, stationwise Moho depth results obtained by the method of Zhu & Kanamori (2000) from *P*-RF are available for subregions of our study area. For the western-central Alps, Moho depths and v_P/v_S ratios are given by Lombardi *et al.* (2008) and compared to active seismic results. We analysed 18 of the stations featured in that study. Wilde-Piórko *et al.* (2005) report Moho depths obtained by three different methods from *P*-RF for 10 stations in the BM as well as Poisson ratios, and co-located Moho depth estimates from seismic studies. Here, we only use the Moho depths obtained by the method of Zhu & Kanamori (2000) for comparison, as all three methods in most cases lead to very similar results for this parameter.

Our picked Moho delay times show good agreement with those of Geissler *et al.* (2008), with a mean difference of 0.16 ± 0.41 s (Figs 12a and d). However, there are four outliers with large differences exceeding 0.5 s, up to a maximum of 2.3 s. In two of these cases, namely stations BRNL and NRDL, which show differences larger than 2 s, both studies identified different phases as Moho phase. The data of these stations show three strong positive phases within the first 6 s (Fig. 13), probably related to sedimentary reverberations, as was already remarked by Geissler *et al.* (2008). Geissler *et al.* (2008) associated the largest phase with the Moho, leading to rather small traveltimes of 3.3 and 2.0 s (Fig. 13), and estimated Moho depths of 26 and 20 km, respectively, which were marked as questionable by the authors and are indeed very shallow

for the station locations. The actual Moho phase at these stations might be masked by the sedimentary phases, which could also explain why the delay time of the Moho phase in *S*-RFs lies between the values obtained from *P*-RF in this study and by Geissler *et al.* (2008) at station NRDL. However, a more detailed investigation would require numerical modelling and is beyond the scope of this study. The other two outliers, on the order of 0.5 s, are associated with the stations JAVC and MUD, which show broad Moho phases that might have been sampled in a different way by the events selected in the two studies (Fig. 13). Actually, Moho depths obtained for station JAVC by the method of Zhu & Kanamori (2000) are within 0.5 km of each other between both studies.

Moho depth estimates likewise broadly agree between our study and that of Geissler *et al.* (2008), with a mean difference of 0.35 ± 3.17 km (Fig. 12b and e). Differences in this range can be attributed to the use of different average crustal velocities in stacking (Grad & Tiira 2012). Outliers with differences larger than 5 km can again be linked to stations on top of thick low-velocity sediments in northern Germany (GSH, NRDL) and stations within the south-eastern Austrian Alps (KBA, OBKA) that show a complicated phase structure (Bianchi *et al.* 2013), maybe related to the recording of phases from both the Adriatic and European Moho. It has also to be noted that the Moho depth estimate for NRDL was not obtained by application of the method of Zhu & Kanamori (2000) by Geissler *et al.* (2008), but by using the picked delay time of 2.0 s and a standard v_P/v_S of 1.73.

The Moho depths obtained in regional studies in the Alps (Lombardi *et al.* 2008) and the BM (Wilde-Piórko *et al.* 2005) show even greater conformity to our results (Fig. 12g). These studies also list active seismic results for the station locations, which show somewhat larger deviations than the RF results among themselves, but are still within 5 km of the corresponding RF depth estimates. Lombardi *et al.* (2008) elaboratedly discuss the problems in applying the method of Zhu & Kanamori (2000) to dipping layers and the resulting bias in depth and v_P/v_S estimates. Their results include corrections for these biases, based on dip estimates from a previously available Moho model from active seismics. For most of the stations that we also analysed in our study, these dip corrections to Moho depth are zero (10 out of the 18 stations) or smaller than 1.5 km (an additional four stations), as we only considered the northern part of the Swiss Seismological Service's network, away from the strongest bending of the Moho beneath the Alps. The big exception is station WTTA in Austria, where the correction applied by Lombardi *et al.* (2008) amounts to 4.5 km. This is also the station with the largest Moho depth in the jointly covered data set and the station where our estimated standard deviation is so large as to prevent further use of the station in our analysis (white circle in Fig. 12g). For this station, the Moho depth estimate from active seismics is actually rather close to our estimated depth, whereas the difference between our depth estimate and that of Lombardi *et al.* (2008) is 4.9 km, and thus nearly identical to the correction they applied.

Finally, obtained v_P/v_S ratios also correlate well between our study and previous ones. The mean difference between our estimates and that of Geissler *et al.* (2008) is 0.003 ± 0.037 (Fig. 12c and f). Remarkably, the two stations with the largest differences (DOU, ARSA) at the same time lead to very similar results, within 1 km, for the Moho depth. Again, variations could be related to the use of different average crustal velocities in stacking and to the additional use of semblance weighting in our study. In comparing our results to the study of Lombardi *et al.* (2008), it is striking that their v_P/v_S ratios are generally a little smaller than our estimates, whereas the results for the BM (Wilde-Piórko *et al.* 2005) agree nearly perfectly
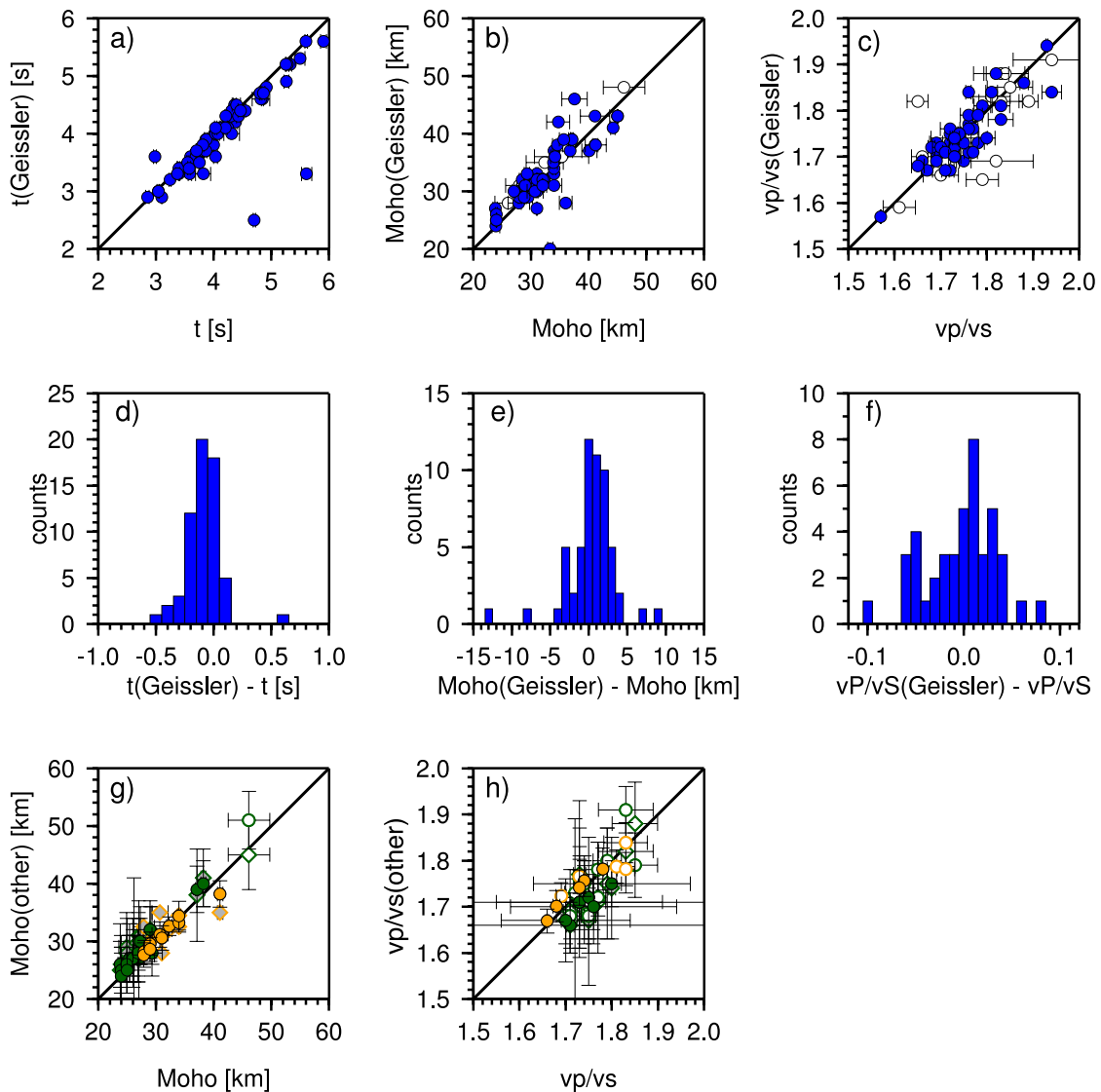
Figure 12. Comparison between our *P*-RF results and those of previous studies at the same stations. (a) and (d) Picked Ps delay time of the Moho phase compared to results of Geissler *et al.* (2008), (b) and (e) Moho depth from Zhu & Kanamori (2000) method compared to results of Geissler *et al.* (2008), (c) and (f) v_P/v_S ratio from Zhu & Kanamori (2000) method compared to results of Geissler *et al.* (2008), (g) and (h) same as (b) and (c) for the studies of Lombardi *et al.* (2008) (green) and Wilde-Piórko *et al.* (2005) (orange). Circles indicate comparison of the RF results, while diamonds give values from active seismics reported in the studies. For the results of the present study, standard deviations from bootstrapping are given by horizontal bars in (a), (b), (c), (g) and (h). Vertical bars in (g) and (h) indicate standard deviations given by Lombardi *et al.* (2008) and Wilde-Piórko *et al.* (2005) for their results. White circle in (b), (c), (g) and (h) and white diamonds in (g) and (h) mark stations with standard deviations larger than 7.5 per cent of Moho depth and larger than 0.01 in v_P/v_S in our results, respectively, that were not used for further interpretation. These data are neither included in (e) and (f).

(Fig. 12h). One could be tempted to relate this to the dip correction, which is negative in the case of the v_P/v_S ratio, except that for most of the stations compared here (10 out of 18), the correction is 0.0 or −0.01, that is extremely small. All observed differences are within the rather large error estimates for v_P/v_S.

4.2 Comparison of Moho maps

General features of our Moho depth map (Fig. 7) agree well with previous observations, for example the distinct increase in Moho depth across the TESZ (e.g. Grad *et al.* 2003a), towards Scandinavia (e.g. Ansorge *et al.* 1992; Gossler *et al.* 1999), and beneath the Alps (e.g. Lombardi *et al.* 2008; Di Stefano *et al.* 2011; Spada *et al.* 2013). We can obtain a more quantitative evaluation, though, by directly comparing our map with the one presented by Grad

et al. (2009). Here, we find close agreement in Germany, Belgium, the Netherlands, the Czech Republic, Eastern Poland and Lithuania (Fig. 14a). For the Czech Republic, Poland and the Baltic countries, Grad *et al.* (2009) mainly rely on seismic and gravity profiles, whereas for Germany, a compilation of refraction seismic data was used. In general, we would not expect perfect agreement between Moho depth estimates based on different methods, like reflection and refraction seismics and RFs (see also Hrubcová & Geissler 2009; Grad & Tiira 2012, for more thorough discussions). For example, both methods work in different frequency ranges, with seismic data using significantly higher frequencies than RFs, in which gradual velocity transitions have different effects. The methods also use different wave types, that is reflected and refracted P-phases versus transmitted Ps or Sp conversions. Both have a different spatial sampling and thus would respond differently to dipping structures.
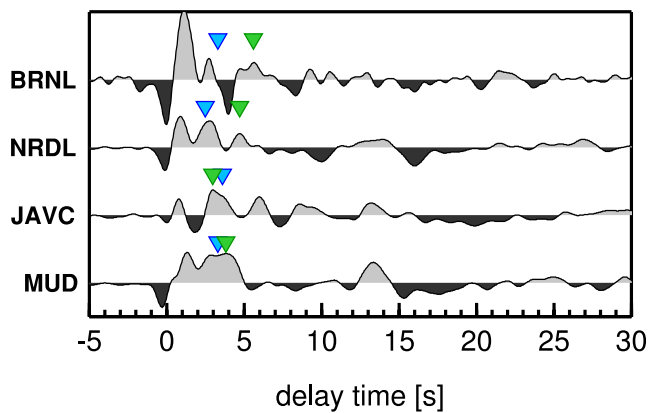
Figure 13. Moveout-corrected *P*-RF sum traces for the four stations that show the largest differences in Moho delay times between our study and the one of Geissler *et al.* (2008). Green triangles mark the Moho delay times picked in our study, while blue triangles denote the delay times given by Geissler *et al.* (2008). See discussion in the text for interpretation of the differences.

Crustal anisotropy can also affect the measurements in different ways. Accordingly, the observed small deviations in the mentioned areas are quite satisfactory. Larger variations, for example along 52°N across Germany, are small-scale and can be attributed to the different level of smoothing between the two maps, where our maps contains more high-frequency information. Larger scale differences are found along 6°E, along the Alpine front from Switzerland to Austria, within western Poland, and in parts of the EEC.

The narrow line of decreased Moho depths compared to Grad *et al.* (2009) along 6°E between 48.5°N and 51°N is caused by shallow Moho depth within the Eifel plume region in our data set. Because of the dense station coverage in this area, we believe that the anomaly is well resolved by our data (Figs 4 and 7a), but might be lost in the map by Grad *et al.* (2009) due to the larger degree of smoothing. In fact, a small-scale crustal thinning to 28 km around 7°E, 50°N was already observed in migrated RFs of the original Eifel Plume Project study (Budweg *et al.* 2006), and corresponding Moho delay times between 3.0 and 3.2 s are obtained in this region by a recent *S*-RFs study (Seiberlich *et al.* 2013).

The sharp increase to Moho depths in excess of 45 km beneath the Alps is located distinctly more to the North in the map of Grad *et al.* (2009). However, their data set actually includes no measurements in Switzerland, where the Moho depth uncertainty correspondingly is up to 7 km. Indeed, our results along the Alpine arc give a close match to recent, more detailed Moho depth maps of the European, Adriatic and Thyrrhenian plates (Di Stefano *et al.* 2011; Spada *et al.* 2013) based on numerous seismic data sets and RFs not included in the work of Grad *et al.* (2009). An exception is the most south-easternly part of the Alps (close to 14°E, 46°N), where Moho depths in excess of 50 km are spuriously introduced in our map by interpolation (compare Figs 7a and b). Besides, our analysis does not include the effect of a dipping Moho on the results obtained by the method of Zhu & Kanamori (2000). Correcting for this effect would potentially increase the Moho depth beneath Austria, where we expect a significant Moho dip (Lombardi *et al.* 2008), and thus further decrease the discrepancy in this region.

Within western Poland, along 16°E, we find a region of increased Moho depth of more than 35 km between 51°N and 53°N that is not contained in the map by Grad *et al.* (2009), whereas Moho depth of less than 30 km are found to the south. This could again reflect some small-scale variability that is smoothed over in the

map by Grad *et al.* (2009), as the larger Moho depths are very likely mostly due to anomalous results at a single station (PB47, blue circle around 17°E, 52°N in Fig. 7a). Besides, Moho depth estimates from RFs could be biased by the slow sediments of the Polish Basin in this region. Thick sediments that are not accounted for result in overestimation of the crustal thickness (Yeck *et al.* 2012). We did try to account for the sediments of the Polish Basin by using a regional velocity model that includes the slow *P*-wave velocities of the sediments. Still, the pronounced 2-D structure of the Basin, with a very sharp eastern boundary as imaged by seismics (Grad *et al.* 2003a), could mean that direct phases and multiples sample different crustal velocity structures in this region. As the method of Zhu & Kanamori (2000) implicitly assumes a 1-D velocity structure, this would bias the results.

Within the EEC, data points within Sweden, Estonia and western Russia show larger Moho depths compared to the map by Grad *et al.* (2009), whereas a single data point off the coast of Latvia points to shallower Moho there. In general, the RF coverage in this region is low, and the depth errors given for this regions by Grad *et al.* (2009) are comparatively high, around 5 km, as their coverage also relies mainly on interpolation in this area. Denser passive seismic networks as well as active studies would be needed to resolve the reason for the observed discrepancies in this region.

In a stationwise comparison between *P*-RF Moho depth estimates and values obtained from the map of Grad *et al.* (2009), we obtain a mean difference of 0.91 ± 3.39 km (Fig. 14b). Outliers with differences larger than 5 km are located in the regions discussed above, for example the Alpine front, Eifel area or Polish Basin. In contrast to the observations by Grad & Tiira (2012), we find only a slight systematic deviation between Moho depths from *P*-RF and those given in the map of Grad *et al.* (2009), with RFs leading to shallower estimates for Moho depth smaller than 30 km and deeper estimates for Moho depth larger than 40 km. Whereas Grad & Tiira (2012) find a linear trend with a slope of 0.61 for the correlation between mapped Moho depth after Grad *et al.* (2009) and Moho depths from RFs, in the present study, the slope is markedly increased to 0.77. As pointed out by Grad & Tiira (2012), this systematic discrepancy is most likely due to the use of global standard velocity models when deriving Moho depth from RFs. Our study corroborates this conclusion as we could significantly reduce the difference by using regional crustal *P*-wave velocities.

Comparing binwise *S*-RFs Moho depth estimates to the data of Grad *et al.* (2009) results in a somewhat different picture, with a mean difference of 2.00 ± 3.73 km. A non-zero mean is already obvious from the corresponding histogram (Fig. 14c). For the Sp data set, we indeed find a trend towards smaller Moho depth estimates compared to Grad *et al.* (2009) for values below 35 km, and larger estimates for values above 45 km (slope of 0.70 in the linear relation). As the majority of our Sp data points is situated in areas with Moho depth of less than 35 km on the map by Grad *et al.* (2009), this explains the shift of the distribution to positive values in Fig. 14c. The likely cause of this trend in *S*-RFs, which is more prominent than in the *P*-RF, is that the used average crustal *S*-wave velocities are less accurate than the *P*-wave velocities. First, detailed models from regional studies like those presented in Karousová *et al.* (2012) and Majdański (2012) only cover *P*-wave velocities, so we had to resort to the less detailed EPcrust (Molinari & Morelli 2011) as our only source of information. Secondly, the *S*-wave velocities within EPcrust are not directly measured quantities, but were determined by applying a scaling relation with respect to the actually measured *P*-wave velocities. Average crustal v_P/v_S ratios accordingly show little variation and lie between 1.70 and 1.75 in the region of this
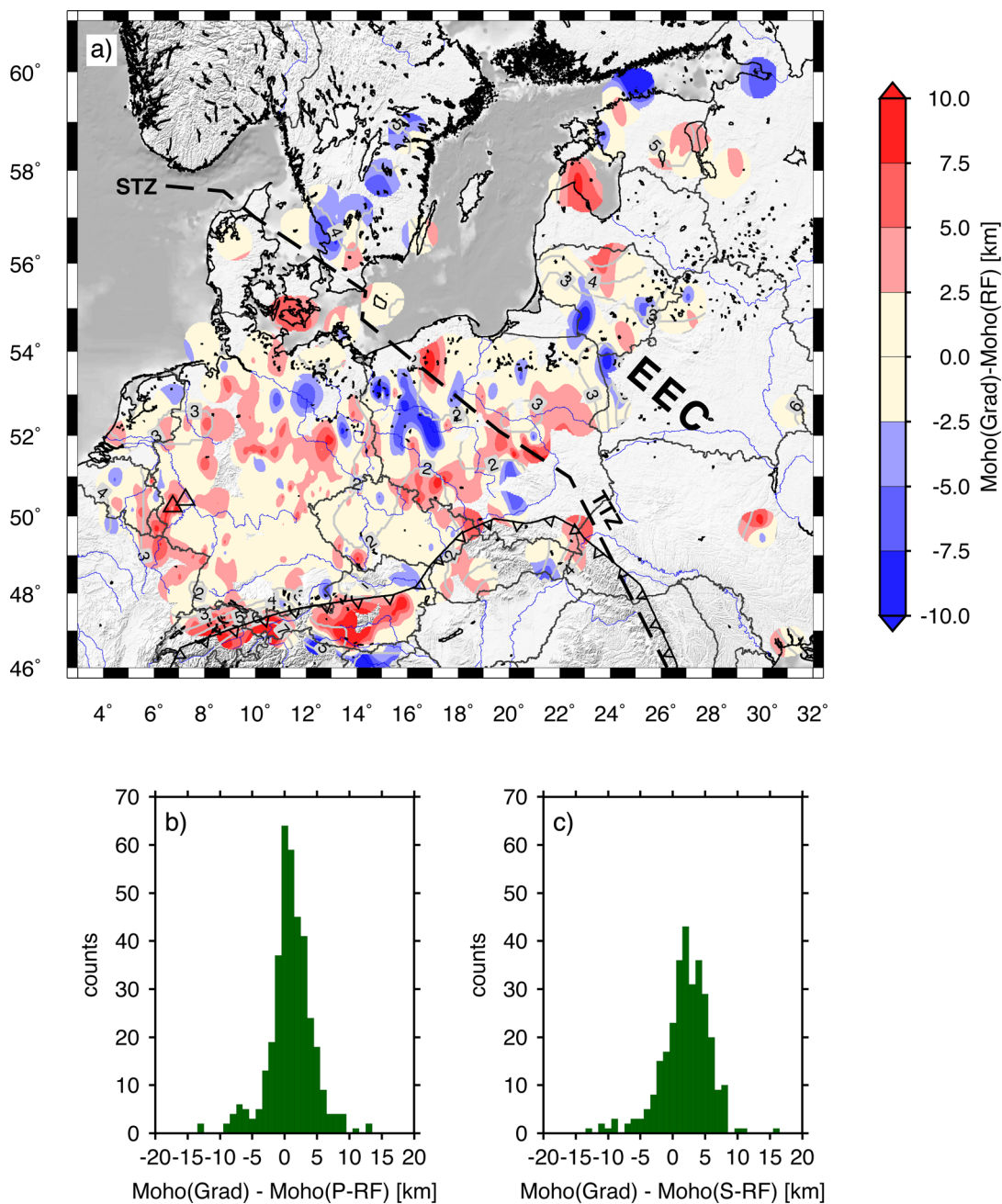
Figure 14. (a) Difference between the Moho depth map by Grad *et al.* (2009) and the map presented here (Fig. 7b) for the area covered by both data sets. Grey contour lines give Moho depth uncertainty in the study of Grad *et al.* (2009). STZ–TTZ, EEC, Alpine-Carpathian Front and location of Quarternary volcanoes in the Eifel area are indicated. (b) Difference between Moho depth values (standard deviation of RF-Moho depths less than 7.5 per cent) at individual stations for *P*-RF. (c) Same as (b), for bins sampled by *S*-RFs.

study. We thus believe that the available *S*-wave velocities do not capture the whole variability in the study area and that the use of independently measured crustal *S*-wave velocities would help to reduce the systematic deviation we find between our *S*-RFs results and the Moho depth map of Grad *et al.* (2009).

4.3 Comparison along POLONAISE'97 profile P4

Comparison of *P*-RF migrated along the POLONAISE'97 profile P4 show a good agreement with the seismic interpretation regarding Moho topography (Fig. 15). Moho depths in Phanerozoic Europe

agree almost perfectly, with a maximum difference of 2 km between the migrated images or the Zhu & Kanamori (2000) results and the seismic model. However, a small scale variation around −60 km along the profile is not resolved by the RFs. This could be due to the smoothing applied during the projection and the fact that a larger area is sampled by the RFs, even without any smoothing, as they have larger Fresnel zones due to their lower frequency content. The transition to a thicker crust is also located at the same place in all data sets, between 130 and 330 km along the profile. A first increase to crustal thicknesses of around 35 km occurs between profile kilometre 150 and the TTZ. Whereas the direct conversions agree with a stepwise transition to depth larger than 40 km near
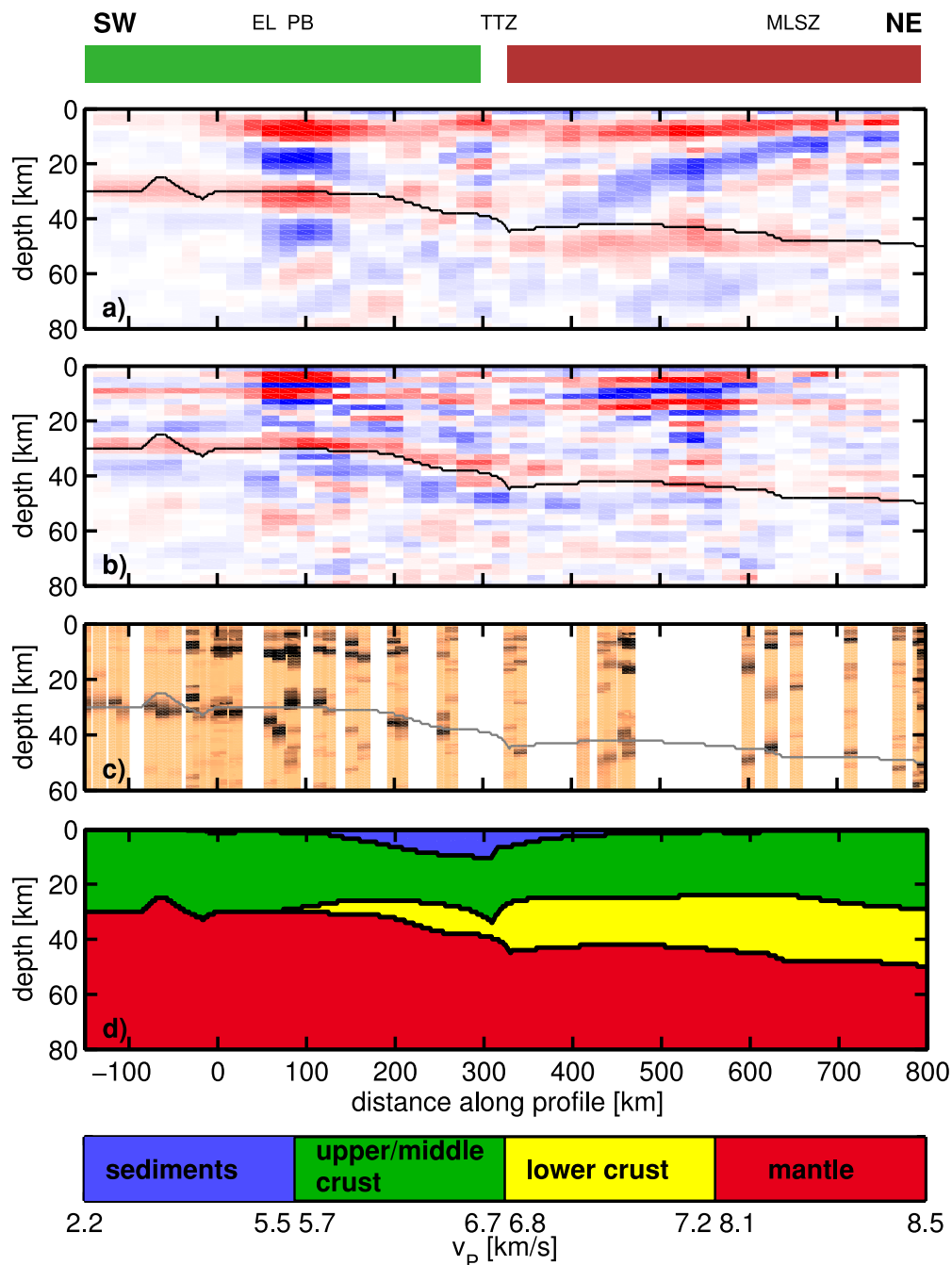
Figure 15. Comparison of RF results with seismic model along POLONAISE'97 profile P4 (Grad *et al.* 2003a). Bar on top provides tectonic information: green for Phanerozoic Europe, red for EEC; EL, Elbe Line; MLSZ, Mid-Lithuanian Suture Zone; PB, Polish Basin; TTZ, Teisseyre-Tornquist Zone. (a) Migrated *P*-RF, (b) summation of migrated PpPs and PpSs multiples, (c) Results from method of Zhu & Kanamori (2000) applied to *P*-RF along the profile, (d) seismic model. Black and grey lines in (a), (b) and (c) give the Moho surface identified along the seismic profile.

profile kilometre 320 (Fig. 15a), though, the migrated multiples give a smoother image of a gradually dipping Moho (Fig. 15b). This trend is also apparent along profile C–C′, the other profile across the TTZ (Fig. 9a and b). This increased smoothing in the migrated multiples could be caused by their lower frequency content and a larger impact of the discrepancy between the 1-D velocity model used in the migration and the actual strong Moho topography across the TTZ due to the longer crustal ray paths compared to direct conversions. The Moho depth map also favours a stepwise transition from a depth of about 35 km to more than 40 km at the surface location of the STZ–TTZ (Fig. 7).

Within the EEC, differences in Moho depth between seismics and migrated RFs become larger, up to 6 km. Interestingly, the migration projects the Moho to larger depth compared to the seismic model for direct conversions, but to shallower depth for the multiples. This is a direct consequence of using *iasp91* as velocity model for the migration, while within the craton, actually both the average crustal velocities (e.g. Grad *et al.* 2003a, see also Tables S1 and S2) and the v_P/v_S ratio (Fig. 10) are higher than in this reference model. The combined effect of higher crustal velocities and v_P/v_S is a larger delay time for the direct conversion, projected to larger depth in the migration with an incorrect velocity model, and reduced delay times

for both multiples, which are then projected to shallower depth in the migration. A more sophisticated migration with an at least 2-D background model should remove this discrepancy, but is beyond the scope of this study. The combined interpretation of migrated direct conversions and multiples at least helps in detecting possible shortcomings of the used velocity model. Consistent with the above explanation, the discrepancy to the seismic model is significantly reduced to less than 2.5 km in the results of the method of Zhu & Kanamori (2000), which combine information from both direct conversion and multiples and use a local velocity model (Fig. 15c).

A dipping structure in the crust is prominently imaged between profile kilometres 350 and 700 in the direct conversions (Fig. 15a). Its negative amplitude implies a velocity decrease with depth. This structure is neither imaged by the multiples (Fig. 15b), nor with *S*-RFs (Fig. 8d), and has no correspondence in the seismic model for profile P4 (Fig. 15d). As discussed in section 4.5 below, this structure is considered an artefact caused by the spurious projection of multiples from a shallow sediment layer.

4.4 Moho topography and crustal properties

Within central Europe, a number of tectonic subdivisions, spanning a broad range of ages, can be traced in the Moho topography. Whereas the TESZ is probably the most prominent feature observed in our map (Fig. 7b), it is by no means the only, or even the oldest, one.

The most ancient tectonic event that has left observable traces in terms of crustal thickness in our area of study affected Lithuania about 1.7 Ga ago (Skridlaite & Motuza 2001). Within Lithuania, we observe a trend towards thicker crust, up to 50 km, in the east, compared to lower crustal thicknesses of less than 45 km in the west (Fig. 7b). This finding correlates with the crustal subdivision of Lithuania along a Palaeoproterozoic terrane boundary into the West Lithuanian Granite Domain as part of the Polish-Lithuanian terrane, and the East Lithuanian Belt as part of the Lithuanian-Belarus terrane (Fig. 1). The two domains are separated by the Mid-Lithuanian Suture Zone, a westward-inclined crustal discontinuity, and have distinctly different metamorphic grades, magnetic and gravimetric properties (Kozlovskaya *et al.* 2001; Skridlaite & Motuza 2001; Bogdanova *et al.* 2006). Although our number of measurement points within Lithuania is limited, there is a clear difference between the median Moho depth obtained west of the Mid-Lithuanian Suture Zone, at 44.3 km, and the one obtained to the east, at 50.2 km. The distinct increase in crustal thickness is also imaged along profile B–B′ at around 24.5°E (Fig. 8f). Interpretation of the EUROBRIDGE seismic profile places the Moho at 42–44 km beneath the West Lithuanian Granite Domain, dipping towards the east and reaching 50 km depth in south-eastern Lithuania (EURO-BRIDGE Seismic Working Group 1999; Yliniemi *et al.* 2001), before descending even further to 55 km within Belarus (Bogdanova *et al.* 2006). This is in good agreement with our results, which furthermore indicate that the Mid-Lithuanian Suture Zone coincides with a change in crustal thickness across all of Lithuania. In contrast to the significant tectonic overprinting that occurred in Phanerozoic Europe, no major deformation event has affected this region of the EEC after the original amalgamation, preserving the contrast in crustal thickness across the Mid-Lithuanian Suture Zone.

The terranes separated by this suture zone are believed to extend into Poland, Latvia, Estonia, Belarus, Russia and Scandinavia (Bogdanova *et al.* 2006). However, we cannot map their contrast in crustal thickness so far. To the north of Lithuania, our coverage is sparse and based on a few broad-band stations, for which we obtain crustal thicknesses of generally less than 50 km within Estonia. Towards the south, in eastern Poland, we find Moho depth between 40 and 45 km, comparable to the POLONAISE'97 results (Czuba *et al.* 2001; Grad *et al.* 2003a), and no west-east increase.

The area covered by the approximately 30–50 km wide Mid-Lithuanian Suture Zone seems to correlate with an area of decreased relative amplitudes in the Moho conversions (Fig. 11), which results in a broadening of the peak in the histogram for region F compared to other cratonic regions, for example in Estonia (region G) or Sweden (region H). The Moho amplitudes show no characteristic difference between the West Lithuanian Granite Domain and the East Lithuanian Belt, though seismic data have shown that the two terranes have markedly different crustal structures, with an about 20 km thick and distinct high-velocity lower crust in the east (Yliniemi *et al.* 2001; Bogdanova *et al.* 2006). If this layer continues within the Lithuania-Belarus terrane into Estonia, the smaller velocity contrast across the Moho could explain the reduced amplitudes of the Moho Ps conversions observed in this region (Fig. 11). A thick mafic lower crustal layer beneath the craton would also result in a higher crustal Poisson's ratio compared to Phanerozoic Europe, as observed in Fig. 10 and discussed by Zandt & Ammon (1995). Fig. 10 actually provides some evidence for higher Poisson's ratios in the east of Lithuania (>0.29), compared to the west (≈0.264), which agrees with the absence or presence of a thick, high-velocity lower crust according to the interpretation of the EUROBRIDGE profile (Yliniemi *et al.* 2001; Bogdanova *et al.* 2006). However, our data coverage in this area is rather sparse in terms of Poisson's ratios and more observations are needed to come to a reliable interpretation.

The TESZ marks a clear contrast in Moho depth (Fig. 7) as well as in Poisson's ratio (Fig. 10), and also in Moho phase amplitude in the *P*-RF (Fig. 11). The increased crustal Poisson's ratio east of the TTZ, with an average value of 0.27, can be attributed to a more mafic composition of the crust, as observed before for platforms and shields (Zandt & Ammon 1995). This observation was not possible with previous data sets (Geissler *et al.* 2008) and can be explained by the presence of a thick, high-velocity lower crust, as observed beneath the Eastern Lithuanian Belt, that was imaged along the POLONASIE'97 seismic profile lines P4 and P5 east of the TTZ (Fig. 15d). The change in Moho phase amplitudes across the STZ–TTZ is probably mostly due to the change in sedimentary cover. Moho phase amplitudes within Poland and Lithuania are larger than, for example, within the BM to the west, whereas the changes in crustal structure, with a fast mafic lower crustal layer beneath the EEC, should have the opposite effect. West of the TTZ lie the thickest sediments of the North Polish Basin (Fig. 17), which, through reverberations and amplification, result in the highest Ps amplitudes observed in our data set. It is questionable, though, whether the high amplitude phases in all cases really represent the Moho (compare Fig. 3). A thinner, but still present, sedimentary cover (Figs 17 and 18), together with the competing effect of a mafic lower crust, can explain the decreasing Moho phase amplitudes across the Baltic countries. While the thick, high-velocity lower crustal layer decreases the velocity contrast across the Moho and thus the amplitudes of the Moho phase, the sediments tend to increase Moho phase amplitudes. With decreasing thickness of sediments, towards a purely crystalline crust beneath Sweden, the Moho phase amplitudes decrease. They are, however, still higher than in the BM for northern Poland and Lithuania, as the BM has a much smaller velocity contrast across the shallowest interface, although the velocity contrast at the Moho is larger due to no fast lower crust.

Continuing south-westward from the TTZ towards northern Germany and southern Poland, the map shows a change from crustal thicknesses greater than 30 km to thicknesses of less than 30 km roughly parallel to the TTZ, but offset to the southwest by some 300 km (Fig. 7b). A corresponding change in Moho depth can also be found along profiles A–A′ (Fig. 8a) and C–C′ (Fig. 9a) at about 16°E and 12°E, respectively. Its location closely coincides with the Elbe Line (EL), which marks a deep crustal boundary that separates a zone of significantly higher lower crustal *P*-wave velocities of 6.9 to 7.2 km s^{-1} to the north-east from lower velocities of less than 6.5 km s^{-1} to the south-west (Aichroth *et al.* 1992; Rabbel *et al.* 1995). Magnetic properties (Bosum & Wonik 1991), crustal reflectivity (Bayer *et al.* 1999) and lower crustal densities (Bayer *et al.* 1999; Scheck *et al.* 1999) also change from one side of the EL to the other. Legendre *et al.* (2012) have recently presented evidence from surface wave tomography that the EL actually extends into the mantle lithosphere. Comparison of the average Moho depth between the EL and the TTZ with the average Moho depth found within an equally sized region to the southwest of the EL leads to values of 32.4 versus 29.3 km, with standard errors of 0.55 and 0.29 km, respectively. While the difference of the average values is only 3 km, it is still significant when regarding the standard errors (Press *et al.* 1992b). Likewise, a Kolmogorov-Smirnov test at a significance level of 1 per cent indicates that the distributions of Moho depth values in the two regions are significantly different. A very similar change in crustal thickness across the EL is found in velocity-depth profiles from seismics (Rabbel *et al.* 1995), and has also been imaged in *P*-RF along the TOR profile in northern Germany (Gossler *et al.* 1999), corroborated by RF inversion (Wilde-Piórko *et al.* 2002). The high-frequency oscillations in Moho depth imaged between the EL and the TTZ, in contrast to a much smoother trend to the southwest, though based on signals observed at single stations, could be an actual feature of the data. Sudden, step-wise, small-scale changes in Moho depth were previously documented in seismic profiles east of the EL, compared to smooth variatios in the west (Aichroth *et al.* 1992; Brink *et al.* 1992). Our data provide additional evidence that the EL marks a change in—at least—crustal structure along its whole extent from northern Germany to the Alpine-Carpathian Front in Poland. Furthermore, the stepwise increase in crustal thickness between Phanerozoic Europe and the EEC, from 29 to 32.5 km east of the EL, to 40 km east of the TTZ, to more than 45 km in eastern Lithuania (Figs 7b, 8a, 9a), together with the recently reported transitional nature of the lithosphere between the EL and the EEC (Legendre *et al.* 2012), agree with the idea of a 'soft' collision along the TESZ during the Variscan orogeny, as proposed by Grad *et al.* (2003a) to explain the limited deformation of pre-Permian strata in the Polish Basin.

Within Phanerozoic Europe, most of the observed Moho structure is due to the most recent tectonic developments. No distinct variations in crustal thickness and properties are imaged along the terrane boundaries of the more distant Caledonian and Variscan orogenies due to more recent overprinting, with the exception of the BM. Here, Moho depth is increasing towards the south, from around 30 km to more than 35 km, as has previously been observed in local RF studies (Geissler *et al.* 2005; Heuer *et al.* 2006), as well as in seismic data (Hrubcová *et al.* 2005). The thickest crust, with a maximum obtained Moho depth of about 41 km at station KHC, is confined to the Moldanubian part of the Massif. A similar and rather abrupt increase in lithospheric thickness below the BM from north to south has been deduced from *S*-RFs (Heuer *et al.* 2007) and from *P*-wave residual spheres (Plomerová *et al.* 2012), which also indicate different lithospheric fabric within the different domains

(Babuška & Plomerová 2013). Heuer (2006) additionally reports systematic variations in v_P/v_S ratios between the different units of the BM, with a decrease from north to south. The values obtained for north-western part of the BM correspond to Poisson's ratios of 0.24 to 0.258 and agree well with the distribution of values in region A of this study (Fig. 10). Furthermore, we observe another north-south variation between the domains that compose the BM, namely a change in Moho phase amplitudes with lower amplitudes found within the Moldanubian and Moravo-Silesian part compared to the Tepla-Barrandian unit (Fig. 11). Higher amplitudes seem to continue to the north-west into the Saxothuringian domain. This result differs from a previous seismic study that found a rather pronounced Moho with a strong velocity contrast beneath both the Moldanubian and Tepla-Barrandian unit, whereas the Saxothuringian showed a highly reflective, laminated lower crust and the Moravo-Silesian unit was characterized by a gradient zone above the Moho (Hrubcová *et al.* 2005). For the Saxothuringian, Hrubcová & Geissler (2009) have shown that a gradient zone of 5 km width or less on top of the Moho might explain both RFs and seismic data in this domain, as a thin gradient zone scarcely influences the amplitude of the direct Moho conversion in the RFs. The gradational velocity transition across more than 10 km within the lower crust as interpreted from seismics beneath the Moravo-Silesian domain can explain the lower Moho phase amplitudes found in the southeastern BM, but not the observation of similarly small amplitudes further to the west. The mapping of the transition between regions of different RF amplitudes could be somewhat biased as we attributed the individual RFs to their station location and not to their piercing points at Moho depth. The offset between the two could be as much as 10 km, and we expect a preferential shift to the north-east, where the majority of the used earthquakes are located. Still, this effect is not sufficient to explain the observed differences. Changes in mantle anisotropy beneath the domains could be a potentially important factor, though: While the actual pattern of lithospheric *P*-wave anisotropy is different in each of the BM's domains, the influence on teleseismic *P* waves coming from the north-east is similar within the Moravo-Silesian and Moldanubian unit on the one hand and within the Tepla-Barrandian and Saxothuringian unit on the other hand (Babuška & Plomerová 2013). Positive *P*-wave residuals, meaning slow *P*-wave velocities in the upper mantle, are found in this direction for stations located in southern part of the BM, whereas negative residuals, that is high *P*-wave velocities, are indicated for stations in the north-west. Lithospheric anisotropy could thus contribute to the reduction of the velocity contrast across the Moho for our dominant earthquake source region in the Moldanubian and Moravo-Silesian units, resulting in smaller amplitudes of the Ps conversions at the Moho, while an increased contrast in the Saxothuringian and Tepla-Barrandian units would lead to higher amplitudes there.

In contrast to the growth of the Variscan orogeny, its collapse has left an imprint on the Moho in central Europe that is still visible today. In northern Germany, we find crust thinned to less than 30 km, with minimum values around 27 km, below the North German Basin (Fig. 7). A similarly thinned crust is also apparent beneath the Central and West Netherlands Basins adjacent to the west (Fig. 7). Corresponding updoming of the Moho beneath the North German Basin has been observed in seismic data along the European Geotraverse (Aichroth *et al.* 1992). Besides, the North German Basin, with a sedimentary fill of about 10 km thickness, is characterized by a significantly raised crustal Poisson's ratio (Fig. 10). High values of v_P/v_S have been observed in northern Germany in a previous RF study (Geissler *et al.* 2008), but not directly related to the influence of sediments.

Similar to the formation of the Central European Basin System, the subsequent Cenozoic rifting can be traced at Moho level. Its most pronounced expression in our study area is surely the Rhine Graben, with a Moho as shallow as 25 km at its southern end. A similar shallowing has also been found in other RF studies of the area (Di Stefano *et al.* 2011; Spada *et al.* 2013) as well as in seismic investigations (e.g. Zucca 1984; Gajewski *et al.* 1987). Poisson's ratio in this region agrees well with the average obtained for Mesozoic-Cenozoic orogenic belts by Zandt & Ammon (1995) and shows no discernible influence of sedimentary deposits within the graben (Fig. 10), which are, however, much thinner than those that have accumulated in parts of the Central European Basin System (Molinari & Morelli 2011). Holbock *et al.* (1987) likewise found an average ν of 0.25 over the whole crust from seismic *P*- and *S*-refraction profiles in the upper Rhine Graben. In addition to the Rhine Graben, the smaller Cenozoic Eger Rift in the north-western BM can also be identified by Moho topography. Crustal thinning beneath the western Eger Rift is known from previous RF studies (Geissler *et al.* 2005; Heuer *et al.* 2006), and an accompanying lithospheric updoming has been observed for the upper Rhine Graben (e.g. Seiberlich *et al.* 2013) as well as for the Eger Rift (e.g. Heuer *et al.* 2006; Plomerová *et al.* 2012).

Similar to the thin crust observed in the Eifel region, other regions of Cenozoic an orogenic volcanism in central Europe also seem to be preferentially located in areas of Moho depth of less than 30 km (Fig. 7b). To corroborate this visual impression, we calculated the average Moho depth for the 24 volcanoes located north of the Alpine-Carpathian Front, which is 28.8 km with a standard error of 0.51 km. Then, we drew 10.000 samples of 24 random points within the same area (6°E to 18°E, 47°N to 54°N) and calculated their average Moho depths. The comparison in Fig. 16 indicates that values similar to the observed average Moho depth beneath the volcanoes or smaller are only obtained in 0.5 per cent of the randomly drawn samples, whereas the average mean Moho depth over 24 randomly selected points is 31 km with a standard error
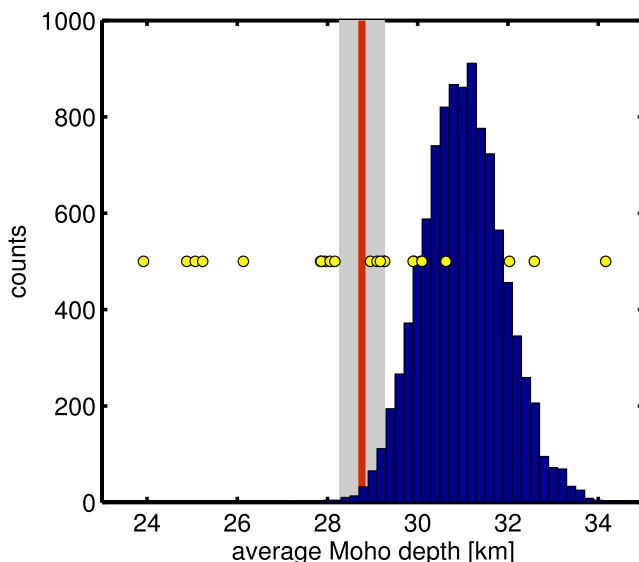
of 0.01 km. We conclude that, while Legendre *et al.* (2012) report that the Cenozoic volcanism in central Europe is located on thin lithosphere above a shallow asthenosphere, our data indicate that the volcanoes are also associated with thinner-than-average crust.

The northern margin of the Alps, as youngest orogeny in our study area, shows up prominently in the Moho topography (Fig. 7) as well as in Ps Moho phase amplitudes (Fig. 11). A drop in Moho depth from 35 km to more than 55 km occurs over less than 100 km laterally along profile D–D' (Fig. 9f). This is significantly more localized than the Moho depth increase across the TESZ, where an increase of 15 km is spread out over 200 km laterally (Fig. 8a), and could either be due to a 'soft' collision across the TESZ to begin with, or to equilibrating mechanisms at work at the much older TESZ, for example crustal alteration, lower crustal flow, or crustal delamination. The high Moho phase amplitudes north of the actual Alpine arc can be explained by amplification within the thick sediments of the Molasse Basin (Fig. 17). The Molasse Basin is also a probable reason for the high v_P/v_S values observed along the Alpine belt in previous RF studies (Geissler *et al.* 2005, 2008), and also indicated here by Poisson's ratios above 0.27 colocated with the high Moho phase amplitudes (compare Figs 10 and 11).

4.5 Crustal structure

To derive additional information on crustal structure, we applied the method of Zhu & Kanamori (2000) to the sediment-basement interface as well as to a possible intra-crustal discontinuity. We used only *P*-RFs in these cases as their higher frequency content leads to a clearer separation between intracrustal and Moho signals, and the identification of shallow phases is hindered in *S*-RFs for stations located on thick sediments by a strong *S*-wave phase at 0 s caused by the use of theoretical angles in the rotation (Fig. 3).

Shallow conversions from a depth of less than 10 km have been found along most of the migrated sections (Figs 8a and f, 9a and f and 15a), and significant sedimentary layers are expected in parts of the study region, for example the Polish Basin, North German Basin and Molasse Basin. When applying the method of Zhu & Kanamori (2000), we used *P*-velocity information from EPcrust (Molinari & Morelli 2011). This model contains an explicit layer of sediments, providing average *P*- and *S*-wave velocities as well as thickness. The other, more detailed regional *P*-wave velocity models (Karousová *et al.* 2012; Majdański 2012) do not designate specific layers as sediments, though they show low velocities in their shallowest part. Our results can directly be compared to the sediment thickness information contained in EPcrust (Fig. 17). Not all stations show clear evidence of a very shallow conversion, and we only display results with bootstrap errors of 0.5 km or less in sediment thickness. Overall, our results show an expected trend, with sediment thicknesses larger than 6 km in the Polish Basin, the North German Basin and the Molasse Basin north of the Alps, and a thin sedimentary cover of less than 3 km in parts of the EEC. However, there is no exact match with the thicknesses from EPcrust. The mean difference between the two values is 0.5 km, with a tendency to larger thicknesses from RFs, but for 90 per cent of the data points, the difference in estimated sediment thickness is less than 3 km. The missing one-on-one correspondence can at least partly be explained by the fact that EPcrust gives sediment thicknesses on a 0.5° × 0.5° grid, whereas our measurements are rather point-like, sampling the subsurface just below the station, where local conditions might differ from an average larger scale value. For example, locally larger values of sedimentary thickness found
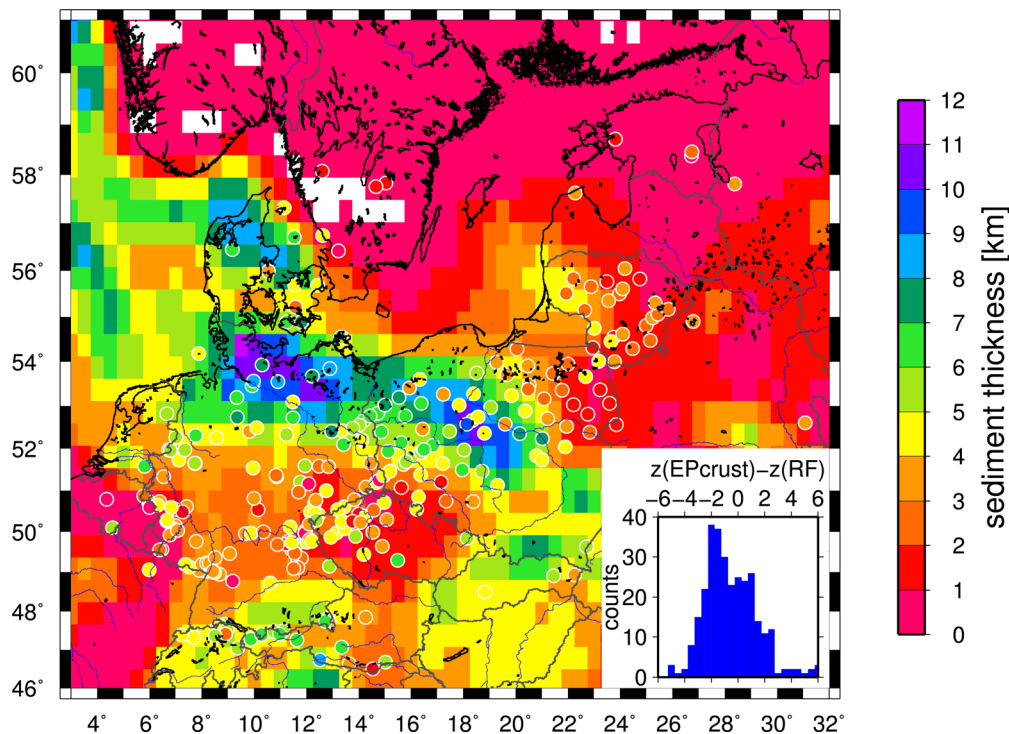

Figure 16. Comparison of average Moho depth beneath 24 Cenozoic anorogonic volcanoes in central Europe with the average Moho depth of 10.000 realizations of 24 random samples selected within the same region (6°E to 18°E by 47°N to 54 °N). Blue histogram represents the results of the 10.000 random selections. Red line with grey error bars denotes the average Moho depth beneath the volcanoes with its standard error, whereas yellow circles are plotted at each of the 24 individual depth values of the volcanoes.

Figure 17. Sediment thickness from EPcrust (Molinari & Morelli 2011), with stationwise measurements obtained from *P*-RF by the method of Zhu & Kanamori (2000) overlain (coloured circles). Only data with an error of less than 0.5 km in sediment thickness from bootstrapping are shown. Inset histogramm at lower right edge of the map shows the difference between the two measurements.

by the RFs might correspond to the sedimentary infill of the Eger Rift (yellow circles in the north-western Czech Republic in Fig. 17) and the Roer Valley Graben (yellow and green circles in the south-eastern Netherlands). Furthermore, specifically within the Polish Basin, the main conversion found in our *P*-RFs might not originate at the sediment-basement interface itself. Along profile POLON-AISE'97 P4, *P*-wave velocities in the sedimentary layer are as high as 5.5 km s^{-1} within a complex stack of high- and low-velocity materials (Grad *et al.* 2003a). The largest velocity contrast might thus not be the one at the lower boundary of this stack, which Grad *et al.* (2003a) find at up to 20 km depth, significantly deeper also than what is described as sediments by EPcrust (Molinari & Morelli 2011). Uncertainties in the used average *P*-wave velocities will also result in depth errors for the sediment-basement contact, and Molinari & Morelli (2011) describe that these velocities sometimes had to be extrapolated from coarser available data. Considering all this, the agreement between our depth estimates and EPcrust is satisfactory.

The most striking crustal feature in the migrated *P*-RFs is the west-ward dipping negative conversion imaged beneath Lithuania and north-eastern Poland (Figs 8a and f, 9a, 15a). There is no similar feature found in the seismic interpretation along POLONAISE'97 profile P4, though (Fig. 15d), or in the migrated multiples (Figs 8b and g, 9b, 15b) or *S*-RFs (Figs 8d and i, 9d). EUROBRIDGE has found a crustal low-velocity zone interpreted as Mesoproterozoic granitic rocks within and to the northwest of the West Lithuanian Granite Domain, however at a nearly constant depth level between 10 and 15 km and with a rather small contrast in *P*-wave velocities of 0.1–0.2 km s^{-1} (Bogdanova *et al.* 2006). Neither the extent nor the depth level and amplitude of the imaged dipping structure can be explained by this zone. Large systems of shear zones spanning the upper and middle crust with substantially lowered *P*-wave velocities due to mylonitization, retrograde recrystallization of granulites and the presence of metasediments have also been reported along the

EUROBRIDGE profile. They are confined to the East Lithuanian Belt (Bogdanova *et al.* 2006), though, whereas the dipping structure is located almost completely to the west of the Mid-Lithuanian Suture Zone. Finally, the suture zone itself is thought to represent a moderately west-dipping, major deformation zone marked by mylonites, along which the West Lithuanian Granite Domain was thrust eastwards onto the East Lithuanian Belt (Skridlaite *et al.* 2003). This could potentially explain the location and polarity of the observed signal. However, the migrated image implies a very low dip of around 5° of the converter. An interface dipping at such a small angle should also be resolvable by *S*-RFs and Ps multiples, though, without being affected by amplitude reductions or polarity reversals (Endrun *et al.* 2005). To explain this discrepancy, we look for other possibilities to explain the imaged feature.

Considering how crustal structure is imaged in general in the *P*-RF sections, it becomes apparent that the crust is nearly transparent at the western ends of profiles A–A′ (Fig. 8a), C–C′ (Fig. 9a) and P4 (Fig. 15a), whereas strong amplitudes, especially negative ones, at depths between 10 and 30 km are found in places where there are significant high-amplitude conversions from the shallow crust. Along profile P4, this applies to the area between profile kilometres 35 and 165, where the profile crosses the Polish Basin, around profile kilometre 290, and between profile kilometres 435 and 750, basically across all of Lithuania. In the case of the Polish Basin, the negative phase at about 20 km depth is readily identified as a sedimentary multiple, as it is a very localized phenomenon and further reverberations continue through the waveform. The multiple arrives at about 2.8 times the traveltime of the preceding positive direct conversion, which can for example be modelled by an average sedimentary *P*-wave velocity of 2.5 km s^{-1} and a high v_P/v_S ratio of 3.5 (Fig. 18a). Assuming a high velocity contrast across the sediment-basement interface is also justified by the very high amplitudes of the shallow conversions, which are larger than the Moho
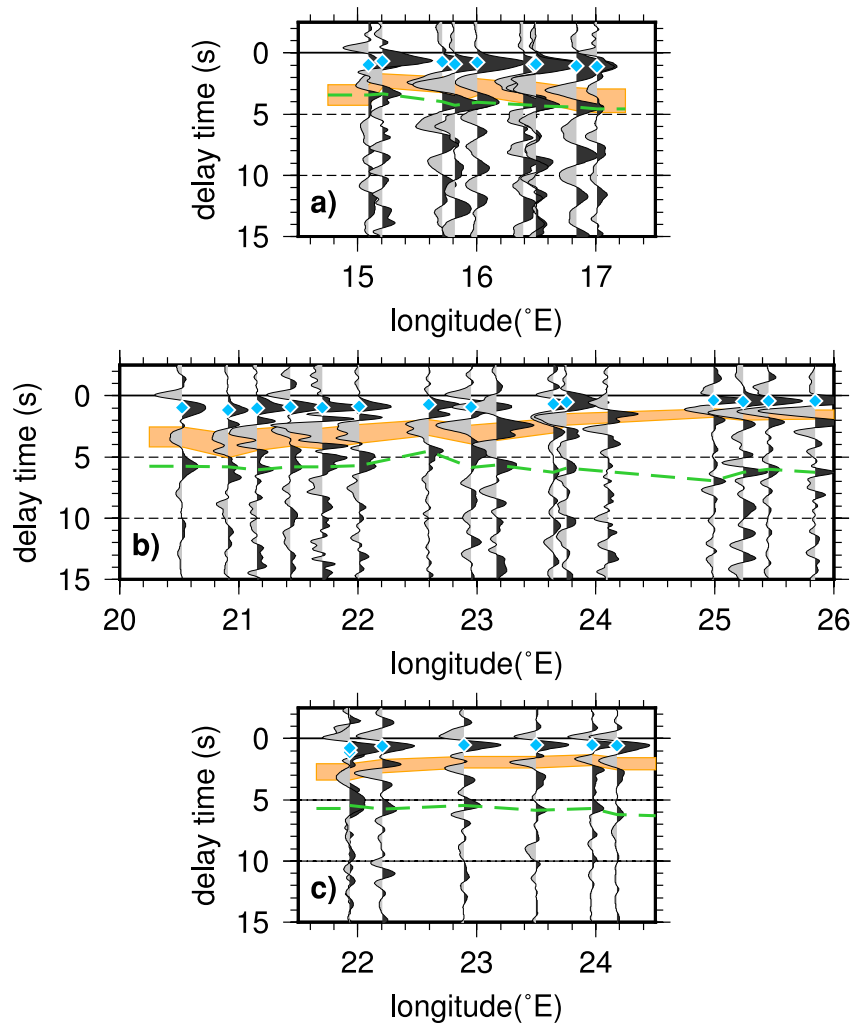
Figure 18. *P*-RF summed by station along parts of profiles A–A′ ((a) Polish Basin, (b) Lithuania) and C–C′ ((c) Lithuania) that show strong negative phases within the crust. Traces are move-out corrected to a slowness of 6.4 s deg^{-1} before stacking. Green dashed line identifies Moho conversion, while blue diamonds indicate delay times of the high-amplitude conversions from shallow sediments. Orange area outlines the range of expected delay times for the second multiple of this conversion, based on a *P*-wave velocity between 2.5 and 4.5 km s^{-1} for the sediments and a v_P/v_S ratio between 3.5 and 1.8.

phases (Fig. 18). The actual timing of the multiples in Fig. 18 is also influenced by the fact that the delay times are indicated on traces move-out corrected for direct conversions, using a velocity model that does not contain the slow sedimentary layer, and that direct conversions and multiples might not sample the exactly same structure. In the case of the dipping structure within eastern Poland/western Lithuania the situation is a little more complex. One has to note, though, that measurements using the RFs themselves as well as EPcrust indicate an increase in sedimentary thickness in Lithuania from east to west, that is towards the Baltic Basin (Fig. 17). The negative conversion that shows increasing delay times to the west follows the same pattern with regard to the proceeding positive signal as in the case of the Polish Basin (Figs 18b and c), that is its delay times can be predicted from those of the direct conversions using a sensible range of values for both average *P*-wave velocities (2.5–4.5 km s^{-1}) and v_P/v_S ratios (1.8–3.5). Thus, it can be explained as a sedimentary multiple and the projection as a dipping crustal structure is an artefact solely due to the increase in sedimentary thickness from east to west along the profiles. As the delay caused by a depth increase of the converter is significantly larger for the multiples compared to the direct conversion, the effect in the

migrated images is also more obvious for the multiples and creates a striking pattern with high negative amplitudes.

After identifying the most pronounced crustal structure as an imaging artefact, we also tried to identify and map conversions at intracrustal depth (i.e. between 10 and 30 km depth) by applying the method of Zhu & Kanamori (2000), using the combined average *P*-wave crustal velocities given by EPcrust (Molinari & Morelli 2011) for the sedimentary and upper crustal layers. In contrast to very shallow layers, for which both direct conversions and multiples are usually separated from the Moho phases, interference with these phases or sedimentary multiples (Fig. 18) may occur for deeper intracrustal discontinuities, complicating their identification. Within Phanerozoic Europe, a clear intracrustal phase is detected only at a small number of randomly distributed stations, as also indicated by the Zhu & Kanamori (2000) results for the Moho (Figs 8c, 9c and f). East of the TTZ, results are somewhat more consistent, and point to a discontinuity at about 15 km depth beneath north-eastern Poland and around 20 km depth beneath Lithuania, which correlates nicely with the transition from upper to middle crust observed in seismics (Yliniemi *et al.* 2001; Grad *et al.* 2003a).

5 CONCLUSION

Our dense RF data set provides information about crustal thickness and structure across central Europe based on homogenous and consistent processing. The excellent agreement with previous *P*-RF studies using a more limited amount of stations and the good correlation with seismic data lend confidence not only to Moho depth estimates from our data set, but also to interpretation of deeper structure, for example the lithosphere-asthenosphere boundary or the mantle transition zone discontinuities (Knapmeyer-Endrun *et al.* 2013), for which no supporting seismic information is available. The use of adequately detailed information on local crustal velocities when applying the method of Zhu & Kanamori (2000) is a prerequisite for a close agreement between seismic and RF estimates of Moho depth. For some regions, for example the Eifel Plume area, and the Swiss Alps, our data also provide more resolution and detail than the previous Moho depth map by Grad *et al.* (2009). We prominently image the TESZ as a stepwise transition in crustal thickness from around 30 km to more than 45 km, spread over 200 km laterally. The EEC is characterized by high Poisson's ratios around 0.27, consistent with a thick mafic lower crust. Additional tectonic domains are resolved within both the EEC and Phanerozoic Europe based on their crustal properties. For example, we detect changes across the Mid-Lithuanian Suture Zone, the EL, and between the Variscan terranes of the BM. Between the Moldanubian and Tepla-Barrandian domain of the BM, thickness changes that we obtain within the crust have been found to encompass the whole lithosphere (Heuer *et al.* 2007; Plomerová *et al.* 2012), whereas the lithosphere between the EL and the TESZ, where we map a Moho depth between that of Phanerozoic Europe and the EEC, was characterized as intermediate between these two tectonic units (Legendre *et al.* 2012). More recent tectonic overprinting, for example the formation of the Central European Basin System and the European Cenozoic Rift System, has erased crustal thickness variations between the different, for example Variscan, domains in Phanerozoic Europe and left its imprint on the Moho in the form of crustal thinning. The decreased thickness of the crust is mirrored by a thinner lithosphere in the European Cenozoic Rift System (Heuer *et al.* 2006; Legendre *et al.* 2012; Plomerová *et al.* 2012; Seiberlich *et al.* 2013), as the spreading is thermally induced. Mapped thickness of the low-velocity surface layer, that is sediments or weathered rock, shows high values of up to 10 km beneath the prominent basins (North German Basin, Polish Basin, Molasse Basin) in the study area, and lowest values of less than 4 km in the EEC, central Germany and the Czech Republic.

ACKNOWLEDGEMENTS

REFERENCES

Aichroth, B., Prodehl, C. & Thybo, H., 1992. Crustal structure along the Central Segment of the EGT from seismic-refraction studies, *Tectonophysics,* **207,** 43–64.

Alinaghi, A., Bock, G., Kind, R., Hanka, W., Wylegalla, K. & the TOR and SVEKALAPKO Working Groups, 2003. Receiver function analysis of the crust and upper mantle from the North German Basin to the Archaen Baltic Shield, *Geophys. J. Int.,* **155,** 641–652.

Ansorge, J., Blundell, D. & Mueller, S., 1992. 3.2 Seismic exploration of the crust along EGT, in *A Continent Revealed—The European Geotraverse,* pp. 35–59, eds Blundel, D., Freeman, R. & Mueller, S., Cambridge Univ. Press.

Artemieva, I., 2011. 3.4 Receiver function (converted waves) studies, in *The Lithosphere – An Interdisciplinary Approach,* pp. 101–114, Cambridge Univ. Press.

Babuška, V. & Plomerová, J., 2013. Boundaries of mantle-lithosphere domains in the Bohemian Massif as extinct exhumation channels for high-pressure rocks, *Gondwana Res.,* **23,** 973–987.

van Balen, R.T., van Bergen, F., de Leeuw, C., Pagnier, H., Simmelink, H., van Wees, J.D. & Verweij, J.M., 2000. Modelling the hydrocarbon generation and migration in the West Netherlands Basin, the Netherlands, *Geol. Mijnb.,* **79,** 29–44.

Banka, D., Pharaoh, T.C., Williamson, J.P. & the TESZ Project Potential Field Core Group, 2002. Potential field imaging of Paleozoic orogenic structure in northern and central Europe, *Tectonophysics,* **360,** 23–45.

Bayer, U. *et al.*, 1999. An integrated study of the NE German Basin, *Tectonophysics,* **314,** 285–307.

Bianchi, I., Bokelmann, G. & Behm, M., 2013. Moho depth & Poisson ratio across Eastern Alps, *Geophys. Res. Abstracts,* vol. 15, EGU2013–5362.

Bogdanova, S. *et al.*, 2006. EUROBRIDGE: new insight into the geodynamic evolution of the East European Craton, in *European Lithospheric Dynamics,* pp. 599–625, eds Gee, D.G. & Stephenson, R.A., Memoir no. 32, Geological Society.

Bosum, W. & Wonik, T., 1991. Magnetic anomaly pattern of Central Europe, *Tectonophysics,* **195,** 43–64.

Brink, H.J., Dürschner, H. & Trappe, H., 1992. Some aspects of the late and post-Variscan development of the Northwestern German Basin, *Tectonophysics,* **207,** 65–95.

Budweg, M., Weber, M., Bock, G., Ritter, J., Christensen, U. & the Eifel-Plume Team, 1999. A 400 km long broad-band antenna in the Eifel region, *ORFEUS Electronic Newsletter,* **1,** 3.

Budweg, M., Bock, G. & Weber, M., 2006. The Eifel Plume – imaged with converted seismic waves, *Geophys. J. Int.,* **166,** 579–589.

Chen, Y., Niu, F., Liu, R., Huang, Z., Tkalčić, H., Sun, L. & Chan, W., 2010. Crustal structure beneath China from receiver function analysis, *J. geophys. Res.,* **115,** B03307, doi:10.1029/2009JB006386.

Christensen, N.I., 1996. Poisson's ratio and crustal seismology, *J. geophys. Res.,* **101,** 3139–3156.

Czuba, W., Grad, M., Luosto, U., Motuza, G., Nasedkin, V. & the POLONAISE P5 Working Group, 2001. Crustal structure of the East European Craton along the POLONAISE'97 P5 profile, *Acta Geophys. Pol.,* **XLIX,** 145–168.

Dadlez, R., Narkiewicz, M., Stephenson, R.A., Visser, M.T.M. & van Wees, J.-D., 1995. Tectonic evolution of the Mid-Polish Trough: modelling implications and significance for central European geology, *Tectonophysics,* **252,** 179–195.

Dadlez, R., Grad, M. & Guterch, A., 2005. Crustal structure below the Polish Basin: is it composed of proximal terranes derived from Baltica?, *Tectonophysics,* **411,** 111–128.

Dézes, P., Schmid, S.M. & Ziegler, P.A., 2004. Evolution of the European Cenozoic Rift system: interaction of the Alpine and Pyrenean orogens with their foreland lithosphere, *Tectonophysics,* **389,** 1–33.

Di Stefano, R., Bianchi, I., Ciaccio, M.G., Carrara, G. & Kissling, E., 2011. Three-dimensional Moho topography in Italy: new constraints from receiver functions and controlled source seismology, *Geochem. Geophys. Geosys.,* **12,** Q09006, doi:10.1029/2011GC003649.

Efron, B. & Gong, G., 1983. A leisurely look at the bootstrap, the jackknife, and cross-validation, *Am. Stat.,* **37,** 36–48.

Endrun, B., Ceranna, L., Meier, T., Bohnhoff, M. & Harjes, H.-P., 2005. Modeling the influence of Moho topography on receiver functions: a case study from the central Hellenic subduction zone, *Geophys. Res. Lett.,* **32,** L12311, doi:10.1029/2005GL023066.

EUROBRIDGE Seismis Working Group, 1999. Seismic velocity structure across the Fennoscandia-Sarmatia suture of the East European Craton beneath the EUROBRIDGE profile through Lithuania and Belarus, *Tectonophysics,* **314,** 193–217.

Farra, V. & Vinnik, L., 2000. Upper mantle stratification by P and S receiver functions, *Geophys. J. Int.,* **141,** 699–712.

Gajewski, D., Holbrook, W.S. & Prodehl, C., 1987. A three-dimensional crustal model of southwest Germany derived from seismic refraction data, *Tectonophysics,* **142,** 49–70.

Geissler, W.H. *et al.*, 2005. Seismic structure and location of a CO_2 source in the upper mantle of the western Eger (Ohře) Rift, central Europe, *Tectonics,* **24,** TC5001, doi:10.1029/2004TC001672.

Geissler, W.H., Kind, R. & Yuan, X., 2008. Upper mantle and lithospheric heterogeneities in central and eastern Europe as observed by teleseismic receiver functions, *Geophys. J. Int.,* **174,** 351–376.

Geissler, W.H., Sodoudi, F. & Kind, R., 2010. Thickness of the central and eastern European lithosphere as seen by S receiver functions, *Geophys. J. Int.,* **181,** 604–634.

Geissler, W.H., Kämpf, H., Skácelová, Z., Plomerová, J., Babuška, V. & Kind, R., 2012. Lithosphere structure of the NE Bohemian Massif (Sudetes)—a teleseismic receiver function study, *Tectonophysics,* **564–565,** 12–37.

Gossler, J., Kind, R., Sobolev, S., Kämpf, H., Wylegalla, K., Stiller, M. & the TOR Working Group, 1999. Major crustal features between the Harz Mountains and the Baltic Shield derived from receiver functions, *Tectonophysics,* **314,** 321–333.

Grad, M. & Tiira, T., 2012. Moho depth of the European Plate from teleseismic receiver functions, *J. Seismol.,* **16,** 95–105.

Grad, M. *et al.*, 2003a. Crustal structure of the Trans-European suture zone region along POLONAISE'97 seismic profile P4, *J. geophys. Res.,* **108,** 2541.

Grad, M., Špičák, A., Keller, G.R., Guterch, A., Brož, M., Hegedüs, E. & SUDETES 2003 Group, 2003b. SUDETES 2003 seismic experiment, *Studia Geophys. Geod.,* **47,** 681–689.

Grad, M., Tiira, T. & the ESC Working Group, 2009. The Moho depth map of the European Plate, *Geophys. J. Int.,* **176,** 279–292.

Gregersen, S. & the TOR Working Group, 1999. Important findings expected from Europe's largest array, *EOS, Trans. Am. geophys. Un.,* **80,** 6.

Guterch, A., Grad, M., Thybo, H., Keller, G.R. & the POLONAISE Working Group, 1999. POLONAISE'97—international seismic experiment between Precambrian and Variscan Europe in Poland, *Tectonophysics,* **314,** 101–121.

Guterch, A. *et al.* 2000 Experiment Team, 2003. CELEBRATION 2000 seismic experiment, *Studia Geophys. Geod.,* **47,** 659–669.

Hamilton, E.L., 1979. V_p/v_s and Poisson's ratio in marine sediments and rocks, *J. acoust. Soc. Am.,* **66,** 1093–1101.

Hansen, S.E., Rodgers, A.J., Schwartz, S.Y. & Al-Amri, A.M.S., 2007. Imaging ruptured lithosphere beneath the Red Sea and Arabian Peninsula, *Earth planet. Sci. Lett.,* **259,** 256–265.

Heuer, B., 2006. Lithospheric and upper mantle structure beneath the western Bohemain Massif obtained from teleseismic P and S receiver functions, Dissertation, FU Berlin, Scientific Technical Report STR 06/12, GeoForschungsZentrum Potsdam.

Heuer, B., Geissler, W.H., Kind, R. & Kämpf, H., 2006. Seismic evidence for asthenospheric updoming beneath the western Bohemian Massif, central Europe, *Geophys. Res. Lett.,* **33,** L05311, doi:10.1029/2005GL025158.

Heuer, B., Kämpf, H., Kind, R. & Geissler, W.H., 2007. Seismic evidence for whole lithosphere separation between Saxothuringian and Moldanubian tectonic units in central Europe, *Geophys. Res. Lett.,* **34,** L09304, doi:10.1029/2006GL029188.

Holbock, W.S., Gajewski, D. & Prodehl, C., 1987. Shear-wave velocity and Poisson's ratio structure of the upper lithosphere in Southwest Germany, *Geophys. Res. Lett.,* **14,** 231–234.

Hrubcová, P. & Geissler, W.H., 2009. The crust-mantle transition and the Moho beneath the Vogtland/West Bohemian region in the light of different seismic methods, *Stud. Geophys. Geod.,* **53,** 275–294.

Hrubcová, P., Środa, P., Špičák, A., Guterch, A., Grad, M., Keller, G.R., Brueckl, E. & Thybo, H., 2005. Crustal and uppermost mantle structure of the Bohemian Massif based on CELEBRATION 2000 data, *J. geophys. Res.,* **110,** B11305, doi:10.1029/2004JB003080.

Hu, J., Xu, X., Yang, H., Wen, L. & Li, G., 2011. S receiver function analysis of the crustal and lithospheric structures beneath eastern Tibet, *Earth planet. Sci. Lett.,* **306,** 77–85.

Jurkevics, A., 1988. Polarization analysis of three-component array data, *Bull. seism. Soc. Am.,* **78**(5), 1725–1743.

Karousová, H., Plomerová, J. & Babuška, V., 2012. Three-dimensional velocity model of the crust of the Bohemian Massif and its effects on seismic tomography of the upper mantle, *Stud. Geophys. Geod.,* **56,** 249–267.

Kennett, B.L.N., Engdahl, E.R. & Buland, R., 1995. Constraints on seismic velocities in the Earth from traveltimes, *Geophys. J. Int.,* **122,** 108–124.

Kieling, K., Roessler, D. & Krueger, F., 2011. Receiver function study in northern Sumatra and the Malaysian peninsula, *J. Seismol.,* **15,** 235–259.

Kind, R., Kosarev, G. & Petersen, N., 1995. Receiver functions at the stations of the German Regional Seismic Network (GRSN), *Geophys. J. Int.,* **121,** 191–202.

Kind, R., Yuan, X. & Kumar, P., 2012. Seismic receiver functions and the lithosphere-asthenosphere boundary, *Tectonophysics,* **536–537,** 25–43.

Knapmeyer, M. & Harjes, H.-P., 2000. Imaging crustal discontinuities and the downgoing slab beneath western Crete, *Geophys. J. Int.,* **143,** 1–21.

Knapmeyer-Endrun, B., Krüger, F., Legendre, C.P., Geissler, W.H. & the PASSEQ Working Group, 2013. Tracing the influence of the Trans-European Suture Zone into the mantle transition zone, *Earth planet. Sci. Lett.,* **363,** 73–87.

Korja, T., 2007. How is the European lithosphere imaged by magnetotellurics?, *Surv. Geophys.,* **28,** 239–272.

Koulakov, I., Kaban, M.K., Tesauro, M. & Cloetingh, S., 2009. P- and S-velocity anomalies in the upper mantle beneath Europe from tomographic inversion of ISC data, *Geophys. J. Int.,* **179,** 345–366.

Kozlovskaya, E.G., Karatayev, G.I. & Yliniemi, J., 2001. Lithosphere structure along the northern part of EUROBRIDGE in Lithuania; results from integrated interpretation of DSS and gravity data, *Tectonophysics,* **339,** 177–191.

Kroner, U. *et al.*, 2008. Variscan tectonics, in *The Geology of Central Europe. Volume 1: Precambrian and Palaeozoic,* pp. 599–664, ed. McCann, T., Geological Society.

Kumar, P., Yuan, X., Kumar, M.R., Kind, R.X., L. & Chadha, R.K., 2007. The rapid drift of the Indian tectonic plate, *Nature,* **449,** 894–897.

Langston, C., 1979. Structure under Mount Rainier, Washington, inferred from teleseimic body waves, *J. geophys. Res.,* **84**(B9), 4749–4762.

Legendre, C.P., Meier, T., Lebedev, S., Friederich, W. & Viereck-Götte, L., 2012. A shear-wave velocity model of the European upper mantle from automated inversion of seismic shear and surface waveforms, *Geophys. J. Int.,* **191,** 282–304.

Levin, V. & Park, J., 2000. Shear zones in the Proterozoic lithosphere of the Arabian Shield and the nature of the Hales discontinuity, *Tectonophysics,* **323,** 131–148.

Li, X., Kind, R., Yuan, X., Wölbern, I. & Hanka, W., 2004. Rejuvenation of the lithosphere by the Hawaiian plume, *Nature,* **427,** 827–829.

Lippitsch, R., Kissling, E. & Ansorge, J., 2003. Upper mantle structure beneath the Alpine orogen from high-resolution teleseismic tomography, *J. geophys. Res.,* **108,** 2376, doi:10.1029/2002JB002016.

Litt, T., Schmincke, H.U., Frechen, M. & Schlüchter, C., 2008. *Quaternary. In: The Geology of Cental Europe, Volume 2: Mesozoic and Cenozoic*, pp. 1287–1340, ed. McCann, T., Geol. Soc., London.

Lombardi, D., Braunmiller, J., Kissling, E. & Giardini, D., 2008. Moho depth and Poisson's ratio in the Western-Central Alps from receiver functions, *Geophys. J. Int.,* **173,** 249–264.

Majdański, M., 2012. The structure of the crust in TESZ area by kriging interpolation, *Acta Geophys.,* **60,** 59–75.

Majorowicz, J. & Wybraniec, S., 2011. New terrestrial heat flow map of Europe after regional paleoclimatic correction application, *Int. J. Earth. Sci.,* **100,** 881–887.

Medhus, A.B., Balling, N., Jacobsen, B.H., Kind, R. & England, R.W., 2009. Deep-structural differences in southwestern Scandinavia revealed by P-wave traveltime residuals, *Norw. J. Geol.,* **89,** 203–214.

Mohorovičić, A., 1910. Potres od 8. X. 1909, *Godišnje izvješće Zagrebačkog meteorološkog opservatorija za godinu 1909, 9/4,* 1–56.

Molinari, I. & Morelli, A., 2011. EPcrust: a reference crustal model for the European plate, *Geophys. J. Int,* **185,** 352–364.

Nikishin, A.M. *et al.*, 1996. Late Precambrian to Triassic history of the East European Craton: dynamics of sedimentary basin evolution, *Tectonophysics,* **268,** 23–63.

Olsson, S., Robert, R.G. & Bödvarsson, R., 2007. Analysis of waves converted from S to P in the upper mantle beneath the Baltic Shield, *Earth planet. Sci. Lett.,* **257,** 37–46.

Paulssen, H., van der Lee, S. & Nolet, G., 1990. The NARS-Netherlands project, *IRIS Newsletter,* **9,** 1–2.

Paulssen, H., Bukchin, B.G., Emelianov, A.P., Lazarenko, M., Muyzert, E., Snieder, R. & Yanovskaya, T.B., 1999. The NARS-DEEP project, *Tectonophysics,* **313,** 1–8.

Pharaoh, T.C., 1999. Paleozoic terranes and their lithospheric boundaries within the Trans-European Suture Zone (TESZ): a review, *Tectonophysics,* **314,** 17–41.

Pharaoh, T.C., Winchester, J.A., Verniers, J., Lassen, A. & Seghedi, A., 2006. The Western accretionary margin of the East European Craton: an overview, in *European Lithospheric Dynamics,* pp. 291–311, eds Gee, D.G. & Stephenson, R.A., Memoir no. 32, Geological Society.

Plomerová, J., Vecsey, L., Babuška, V., Granet, M. & Achauer, U., 2005. Passive seismic experiment MOSAIC – a pilot study of mantle lithosphere anisotropy of the Bohemian Massif, *Stud. Geophys. Geod.,* **49,** 541–560.

Plomerová, J., Vecsey, L. & Babuška, V., 2012. Mapping seimic anisotropy of the lithospheric mantle beneath the northern and eastern Bohemian Massif (central Europe), *Tectonophysics,* **564–565,** 38–53.

Press, W.H., Teukolsky, S.A., Vetterling, W.T. & Flannery, B.P., 1992a. Are two distributions different?, *Numerical Recipes in C,* Chap. 14.3, 2nd edn, pp. 620–628, Cambridge Univ. Press.

Press, W.H., Teukolsky, S.A., Vetterling, W.T. & Flannery, B.P., 1992b. Do two distributions have the same mean or variances?, *Numerical Recipes in C,* Chap. 14.2, 2nd edn, pp. 615–619, Cambridge Univ. Press.

Prodehl, C., Mueller, S. & Haak, V., 2006. The European Cenozoic rift system, in *Continental Rifts: Evolution, Structure, Tectonics,* ed. Olsen, K.H., Developments in Geotectonics no. 25, pp. 133–212, Elsevier.

Rabbel, W., Förster, K., Schulze, A., Bittner, R., Röhl, J. & Reichert, J.C., 1995. A high-velocity layer in the lower crust of the North German Basin, *Terra Nova,* **7,** 327–337.

Reicherter, K. *et al.*, 2008. Alpine tectonics north of the Alps, in *The Geology of Central Europe. Volume 2: Mesozoic and Cenozoic,* pp. 1233–1285, ed. McCann, T., Geological Society.

Ritter, J.R.R., Wagner, M., Wawerzinek, B. & Wenzel, F., 2008. Aims and first results of the TIMO project – Tiefenstruktur des mittleren Oberrheingrabens, *Geotecton. Res.,* **95,** 151–154.

Scheck, M., Barrio-Alvers, L., Bayer, U. & Götze, H.-J., 1999. Density structure of the Northeast German Basin: 3D modelling along the DEKORP line BASIN96, *Phys. Chem. Earth (A),* **24,** 221–230.

Schulmann, K., Konopásek, J., Janoušek, V., Lexa, O., Lardeaux, J.-M., Edel, J.-B., Štípská, P. & Ulrich, S., 2009. An Andean type Palaeozoic convergence in the Bohemian Massif, *C. R. Geosci.,* **341,** 266–286.

Schweitzer, J., 1995. Blockage of regional seismic waves by the Teisseyre-Tornquist zone, *Geophys. J. Int.,* **123,** 260–276.

Seiberlich, C.K.A., Ritter, J.R.R. & Wawerzinek, B., 2013. Topography of the lithosphere-asthenosphere boundary below the Upper Rhine Graben rift and the volcanic Eifel region, Central Europe, *Tectonophysics,* **603,** doi:10.1116/j.tecto.2013.05.034.

Sissingh, W., 1996. Comparative Tertiary stratigraphy of the Rhine Graben, Bresse Graben and Molasse Basin: correlation of Alpine foreland events, *Tectonophysics,* **300,** 249–284.

Skridlaite, G. & Motuza, G., 2001. Precambrian domains in Lithuania: evidence of terrane tectonics, *Tectonophysics,* **339,** 113–133.

Skridlaite, G., Willingshofer, E. & Stephenson, R., 2003. P-T-t modelling of Proterozoic terranes in Lithuania: geodynamic implications for accretion of southwestern Fennoscandia, *GFF,* **125,** 201–211.

Sodoudi, F. *et al.*, 2006. Lithospheric structure of the Aegean obtained from P and S receiver functions, *J. geophys. Res.,* **111,** B12307, doi:10.1029/2005JB003932.

Sodoudi, F., Yuan, X., Kind, R., Heit, B. & Sadidkhouy, A., 2009. Evidence for a missing crustal root and a thin lithosphere beneath the Central Alborz by receiver function studies, *Geophys. J. Int.,* **177,** 733–742.

Spada, M., Bianchi, I., Kissling, E., Piana Agostinetti, N. & Wiemer, S., 2013. Combining controlled-source seismology and receiver function information to derive 3-D Moho topography for Italy, *Geophys. J. Int.,* doi:10.1093/gji/ggt148.

Taghizadeh-Farahmand, F., Sodoudi, F., Afsari, N. & Ghassemi, M.R., 2010. Lithospheric structure of NW Iran from P and S receiver functions, *J. Seism.,* **14,** 823–836.

Tatham, R.H., 1982. V_p/v_s and lithology, *Geophysics,* **47,** 336–344.

Tesauro, M., Kaban, M.K. & Cloetingh, S.A.P.L., 2008. EuCRUST-07: a new reference model for the European crust, *Geophys. Res. Lett.,* **35,** L05313, doi:10.1029/2007GL032244.

Tkalčić, H., Chen, Y., Liu, R., Zhibin, H., Sun, L. & Chan, W., 2011. Multistep modellling of teleseismic receiver functions combined with constraints from seismic tomography: crustal structure beneath southeast China, *Geophys. J. Int.,* **187,** 303–326.

Vinnik, L.P., 1977. Detection of waves converted from P to SV in the mantle, *Phys. Earth planet. Inter.,* **15,** 39–45.

Wehling-Benatelli, S., Becker, D., Bischoff, M., Friederich, W. & Meier, T., 2013. Indications for different types of brittle failure due to active coal mining using waveform similarities of induced seismic events, *Solid Earth,* **4,** 405–422.

White, D.J., Milkereit, B., Salisbury, M.H. & Percival, J.A., 1992. Crystalline lithology across the Kapuskasing uplift determined using in situ Poisson's ratio from seismic tomography, *J. geophys. Res.,* **97,** 19 993–20 006.

Wilde-Piórko, M., Grad, M. & the POLONAISE working group, 1999. Regional and teleseismic events recorded across the TESZ during POLONAISE'97, *Tectonophysics,* **314,** 161–174.

Wilde-Piórko, M., Grad, M. & the TOR Working Group, 2002. Crustal structure variation from the Precambrian to Paleozoic platforms in Europe imaged by the inversion of receiver functions—project TOR, *Geophys. J. Int.,* **150,** 261–270.

Wilde-Piórko, M., Saul, J. & Grad, M., 2005. Differences in the crustal and uppermost mantle structure of the Bohemian Massif from teleseismic receiver functions, *Stud. Geophys. Geod.,* **49,** 85–107.

Wilde-Piórko, M. *et al.*, 2008. PASSEQ 2006-2008: passive seismic experiment in Trans-European Suture Zone, *Stud. Geophys. Geod.,* **52,** 439–448.

Winchester, J.A. & the PACE TMR Network Team, 2002. Paleozoic amalgamation of Central Europe: new results from recent geological and geophysical investigations, *Tectonophysics,* **360,** 5–21.

Wittlinger, G., Farra, V., Hetényi, G., Vergne, J. & Nábělek, J., 2009. Seismic velocities in Southern Tibet lower crust: a receiver function approach for eclogite detection, *Geophys. J. Int.,* **177,** 1037–1049.

Yeck, W.L., Sheehan, A.F. & Schulte-Pelkum, V., 2012. Sequential H-κ stacking to obtain accurate crustal thickness beneath sedimentary basins, *Bull. seism. Soc. Am.,* **103,** 2142–2150.

Yegorova, T.P. & Starostenko, V.I., 1999. Large-scale three-dimensional gravity analysis of the lithosphere below the the transition zone from Western Europe to the East European Platform, *Tectonophysics,* **314,** 83–100.

Yliniemi, J. *et al.*, 2001. EUROBRIDGE'95: deep seismic profiling within the East European Craton, *Tectonophysics,* **339,** 153–175.

Yuan, X., Kind, R., Li, X. & Wang, R., 2006. The S receiver functions: synthetics and data example, *Geophys. J. Int.,* **165,** 555–564.

Zandt, G. & Ammon, C., 1995. Continental crust composition constrained by measurements of crustal Poisson's ratio, *Nature,* **374,** 152–154.

Zandt, G., Myers, S.C. & Wallace, T.C., 1995. Crust and mantle structure across the Basin and Range-Colorado Plateau boundary at 37° N latitude and implications for Cenozoic extensional mechanism, *J. geophys. Res.,* **100**(B6), 10 529–10 548.

Zhu, L. & Kanamori, H., 2000. Moho depth variations in southern California from teleseismic receiver functions, *J. geophys. Res.,* **105**(B2), 2969–2980.

Zhu, H., Bozdağ, E., Peter, D. & Tromp, J., 2012. Structure of the European upper mantle revealed by adjoint tomography, *Nat. Geosci.,* **5,** 493–498.

Ziegler, P.A., 1994. Cenozoic rift system of western and central Europe: an overview, *Geol. Mijnbouw,* **73,** 99–127.

Ziegler, P.A. & Dézes, P., 2006. Crustal evolution of Western and Central Europe, in *European Lithospheric Dynamics,* pp. 43–56, eds Gee, D.G. & Stephenson, R.A., Memoir no. 32, Geological Society.

Zucca, J.J., 1984. The crustal structure of the southern Rhinegraben from re-interpretation of seismic refraction data, *J. Geophys.,* **55,** 13–22.

SUPPORTING INFORMATION

Additional Supporting Information may be found in the online version of this article:

Table S1. Moho depth derived from P-RFs.
Table S2. Moho depth derived from S-RFs.
(http://gji.oxfordjournals.org/lookup/suppl/doi:10.1093/gji/ggu035/-/DC1).

Please note: Oxford University Press are not responsible for the content or functionality of any supporting materials supplied by the authors. Any queries (other than missing material) should be directed to the corresponding author for the article.